

OPEN ACCESS

**Repository of the Max Delbrück Center for Molecular Medicine (MDC)
in the Helmholtz Association**

<https://edoc.mdc-berlin.de/15378/>

MACC1 induces tumor progression in transgenic mice and colorectal cancer patients via increased pluripotency markers Nanog and Oct4

Lemos C., Hardt M.S., Juneja M., Voss C., Foerster S., Jerchow B., Haider W., Blaker H., Stein U.

This is a copy of the accepted manuscript, as originally published online ahead of print by the American Association for Cancer Research. The original article has been published in final edited form in:

Clinical Cancer Research
2016 JUN 01 ; 22(11): 2812-2824
2016 JAN 12 (first published online)
doi: [10.1158/1078-0432.CCR-15-1425](https://doi.org/10.1158/1078-0432.CCR-15-1425)

Publisher: [American Association for Cancer Research](#)

Copyright © 2016 by the American Association for Cancer Research.

MACC1 induces tumor progression in transgenic mice and colorectal cancer patients via increased pluripotency markers Nanog and Oct4

Clara Lemos^{1Ψ*}, Markus S. Hardt^{1,2 Ψ}, Manisha Juneja¹, Cynthia Voss^{1,2}, Susann Förster³, Boris Jerchow³, Wolfram Haider⁴, Hendrik Bläker⁵, Ulrike Stein^{1,2*}

¹Experimental and Clinical Research Center, a joint cooperation between the Charité Medical Faculty and the Max-Delbrück-Center for Molecular Medicine, Robert-Rössle-Straße 10, 13125 Berlin, Germany

²German Cancer Consortium, Im Neuenheimer Feld 280, 69120 Heidelberg, Germany

³Max-Delbrück-Center for Molecular Medicine, Robert-Rössle-Straße 10, 13125 Berlin, Germany

⁴Institute for Animal Pathology, Schönhauser Straße 62, 13127 Berlin, Germany

⁵Institute of Pathology, Charité Medical Faculty, Charitéplatz 1, 10117 Berlin, Germany

Ψ These authors contributed equally to this work.

Running title: MACC1 increases Wnt signaling and pluripotency

Keywords: colorectal cancer; tumor progression; MACC1; Wnt signaling; pluripotency

Grant support: This work was supported by the Alexander von Humboldt Foundation (C.L.), the Wilhelm Sander Foundation (U.S., B.J.), the Monika-Kutzner foundation (U.S.), the German Cancer Consortium (US, C.V. and M.S.H.) and the Preclinical Comprehensive Cancer Center (U.S., C.L.).

*Corresponding authors:

Clara Lemos and Ulrike Stein

Max-Delbrück-Center for Molecular Medicine, Robert-Rössle-Straße 10, 13125 Berlin, Germany

Phone: +49 30 9406 3432; Fax: +49 30 9406 2780;

e-mail: lemosc@gmail.com; ustein@mdc-berlin.de

Disclosure: The authors declare no conflict of interest.

Authors' contributions: C.L. designed and performed experiments, analyzed data and wrote the manuscript. M.S.H. designed and performed all the *in vitro* and patient experiments with pluripotency markers, analyzed data and wrote the manuscript. M.J. contributed to some experiments and critically revised the manuscript. C.V. provided significant technical assistance. S.F. performed bioinformatics analyses. B.J. supervised the pro-nucleus injection. W.H. and H.B. performed all the histopathological analysis. U.S. supervised the project and critically revised the manuscript.

Translational Relevance

The gene MACC1 is an established biomarker for metastasis and survival in colorectal cancer patients. Here, we provide first evidence that MACC1-induced tumor progression acts, at least in part, via the newly discovered MACC1/Nanog/Oct4 axis. The evidence is accumulated from experiments in cell culture, MACC1 transgenic animals as well as colorectal cancer patients. This is the first time that the function of MACC1 is linked to pathways crucial in cancer stem cells. Based on the hypothesis that cancer stem cells are the main engine behind tumor progression and metastasis, these findings might have important therapeutic implications. Specifically, MACC1's relevance as a biomarker might further be augmented by focusing on its expression in cancer stem cells. Furthermore, the connection of MACC1 with Oct4 and Nanog might offer novel options for therapeutic intervention.

Abstract

Purpose: We have previously identified the gene MACC1 as a strong prognostic biomarker for colorectal cancer metastasis and patient survival. Here, we report for the first time the generation of transgenic mouse models for MACC1.

Experimental Design: We generated mice with transgenic overexpression of MACC1 in the intestine driven by the villin promoter (vil-MACC1) and crossed them with Apc^{Min} mice (vil-MACC1/ Apc^{Min}).

Results: vil-MACC1/ Apc^{Min} mice significantly increased the total number of tumors ($P = 0.0056$). This was particularly apparent in large sized tumors (≥ 3 mm diameter; $P = 0.0024$). A detailed histopathological analysis of these lesions demonstrated that the tumors from the vil-MACC1/ Apc^{Min} mice had a more invasive phenotype and consequently, showed a significantly reduced survival time as compared to Apc^{Min} mice ($P = 0.03$). Molecular analysis revealed an increased Wnt and pluripotency signaling in the tumors of vil-MACC1/ Apc^{Min} mice. Specifically, we observed a prominent upregulation of the pluripotency markers Oct4 and Nanog in these tumors as compared to Apc^{Min} controls. Finally, we could also validate that Oct4 and Nanog are regulated by MACC1 *in vitro*, and strongly correlate with MACC1 levels in a cohort of 60 tumors of colorectal cancer patients ($r = 0.7005$ and $r = 0.6808$, respectively; $P > 0.0001$ and $P > 0.0002$, respectively).

Conclusions: We provide proof of principle that MACC1-induced tumor progression in colorectal cancer acts, at least in part, via the newly discovered MACC1/Nanog/Oct-4 axis. These findings might have important implications for the design of novel therapeutic intervention strategies to restrict tumor progression.

Introduction

Worldwide, colorectal cancer (CRC) is one of the most common malignancies with more than 1 million cases diagnosed every year (1). Colorectal carcinogenesis is a multistep process associated with the accumulation of genetic alterations and mutations in oncogenes and tumor-suppressor genes (2). Prominent among these is the tumor-suppressor polyposis adenomatous coli (APC) gene, which is somatically mutated in more than 80% of sporadic colorectal tumors (3). Loss of APC function leads to inappropriate β -catenin stabilization, accumulation in the cytoplasm and translocation to the nucleus, resulting in a constitutively active Wnt signaling. APC mutations, and consequent Wnt signaling activation, is regarded as the initiating event in CRC, playing also an important role in tumor progression (4–6).

MACC1 was identified by our group as a strong prognostic biomarker for CRC metastasis and patient survival (7). MACC1 induces proliferation, migration and invasion of CRC cells *in vitro*, and promotes tumor growth and metastasis in xenograft mouse models (7,8). MACC1 was found significantly upregulated in primary colon cancer and organ metastases compared to normal tissues, indicating that the induction of MACC1 might occur at the crucial step of transition from the benign to the malignant phenotype in the adenoma-carcinoma sequence of CRC (7,9). MACC1 has been described as a prognostic biomarker for tumor progression, metastasis, and survival in different solid tumors (10), including hepatocellular carcinoma (11–19), gastric (20,21), esophageal (22,23), cervical (24,25) and lung cancer (26–28). Met was identified as the first transcriptional target of MACC1, suggesting that MACC1 might signal through the HGF-Met pathway to promote tumor growth and metastasis. In contrast to MACC1, Met was not prognostic for metastasis-free survival in CRC patients. Moreover, the combination of MACC1 and Met expression was not capable of improving the prognostic power of MACC1 alone (7). Therefore, one can anticipate that relevant target genes and/or pathways, other than Met, might be regulated by MACC1 and contribute to the tumor-promoting phenotype associated with MACC1 overexpression.

Considerable evidence has accumulated which suggests that tumors are maintained by dedicated stem cells (29-31). Strikingly, MACC1 has appeared upregulated in the gene expression signature of intestinal stem cells in the mouse (29). However, a connection between MACC1 and stem cell signaling has never been established.

To genetically address the role of MACC1 in intestinal tumorigenesis and to further evaluate the molecular determinants underlying MACC1-associated phenotypes, we generated transgenic mouse

models with intestine-specific overexpression of MACC1, vil-MACC1 and vil-MACC1/Apc^{Min}. Our results show that MACC1 induces tumor progression in an Apc-mutated background. Intriguingly, our findings in cell culture, novel MACC1 transgenic mice as well as in tumors of CRC patients uncover the pluripotency markers Oct4 and Nanog as novel essential signaling mediators used by MACC1 to induce tumor progression.

Materials and Methods

Mice

A sequence containing a chimeric intron, the full length cDNA of human MACC1 and a V5 tag were cloned into the p12.4kbVillin-ΔATG vector (kindly provided by Dr. Deborah Gumucio, University of Michigan), which contains the mouse villin promoter (30). The p12.4kbVillin/int-MACC1-V5 plasmid was confirmed by sequencing. The transgene was isolated from the plasmid by (PmeI) digestion. The linearized and purified transgene was microinjected into fertilized mouse eggs (C57BL/6N) and implanted into pseudopregnant females by the Transgenic Core Facility of the Max-Delbrück-Center for Molecular Medicine (Berlin). The resulting founders and their progeny were genotyped by PCR of tail or ear-tag DNA using transgene-specific (genotyping) primers and mouse beta-globin primers as internal control (supplementary Table 1). Four founder lines were established on a pure C57BL/6N genetic background, [C57BL/6N-Tg(vil-MACC1); T8892, T9757, T9760, T9765; Lab code: Us] Vil-MACC1 transgenic females were crossed with C57BL/6J-Apc^{Min}/J males (Jackson Laboratories) to generate vil-MACC1/Apc^{Min} mice.

Animals were housed in individually ventilated cages in a specific pathogen-free mouse facility at the Max-Delbrück-Center for Molecular Medicine (Berlin). All animal studies were approved by local governmental authorities (Landesamt für Gesundheit und Soziales Berlin, Germany).

CRC subjects and tissues

We obtained tissue specimens from 60 subjects with colorectal cancer with informed written consent (approved by Charité Ethics Committee, Charité Universitätsmedizin, Berlin, Campus Mitte) (31). The 60 subjects had stage 1 to 3 cancer (no distant metastases at the time of surgery), were previously untreated, did not have a history of familial colon cancer, did not suffer from a second tumor of the same or a different entity and underwent surgical R0 resection (complete resection with no microscopic residual tumor). Twenty-three subjects in this group developed distant metastases metachronously (median follow-up, 47.2 months).

Isolation of IECs

Total intestinal epithelial cells (IECs) were isolated from the duodenum, jejunum, ileum and colon by sequential incubation of intestinal tissue in 1 mM DTT and 1.5 mM EDTA solutions as described previously (32).

The sequential isolation of mouse small intestinal epithelial cells along the crypt-villus axis was performed as previously described (33), with minor modifications. Briefly, the small intestines were removed after sacrifice of the mice, open longitudinally, rinsed twice in ice-cold PBS and incubated at 37°C for 15 minutes in a citrate buffer containing 96 mM NaCl, 1.5 mM KCl, 27 mM sodium citrate, 8 mM KH₂PO₄ and 5.6 mM Na₂HPO₄, pH 7.3. The tissues were then transferred to a Falcon tube containing 15 ml PBS buffer with 1.5 mM EDTA (to remove calcium), 0.5 mM DTT, and 1 mg/ml BSA, and placed in a shaking incubator (37°C; 180 rpm) for 10 minutes. The small intestines were removed from the first Falcon, gently shaken to remove adhering enterocytes, and transferred to a second Falcon containing 15 ml of PBS, EDTA, DTT and BSA. This procedure was repeated for a total of nine consecutive incubation steps at 37°C, each step lasting 10, 6, 5, 5, 9, 10, 15, 25 and 30 minutes, respectively. The cells detached during each incubation were collected and immediately centrifuged at 0°C, 1000 g for 3 minutes. The pellets were washed twice in ice-cold PBS and stored at -20°C.

Western Blot

For total protein extraction, cells were lysed with RIPA buffer (50 mM Tris-HCl [pH 7.5], 150 mM NaCl, 1% Nonidet P-40; supplemented with protease and phosphatase inhibitor cocktail tablets [Roche Diagnostics]) for 30 minutes on ice. Protein concentration was quantified with Bicinchoninic Acid Protein Assay Reagent (Pierce), according to manufacturer's instructions, and lysates of equal protein amount were separated with sodium dodecyl sulfate-polyacrylamide gel electrophoresis (SDS-PAGE) and blotted onto Optitran BA-S 85 nitrocellulose membranes (GE Healthcare). Membranes were incubated in blocking solution containing 5 % non-fat dry milk for 1 hour at room temperature, followed by an incubation overnight at 4°C with primary antibodies: rabbit anti-MACC1 (polyclonal, Sigma-Aldrich, dilution 1:1000), rabbit anti-Oct4 (polyclonal, Abcam ab19857, dilution 1:500) and mouse anti-β-actin (clone AC-74, Sigma-Aldrich, dilution 1:20000). Subsequently, the membranes were incubated for 1 hour at room temperature with secondary HRP-coupled antibodies (Promega and Thermo Scientific), developed with WesternBright ECL Western blotting detection kit (Advansta) and visualized in a FluorChem Q imager (Biozym). Immunoblotting for β-actin served as protein loading control.

Chromatin immunoprecipitation (ChIP)

Chromatin immunoprecipitation (ChIP) was carried out according to standard protocols as described previously(34). Cell lysates were sonicated for 15 pulses at 40% output. Incubation with monoclonal V5-specific antibody (Invitrogen) was performed overnight at 4°C. Immunoprecipitation of the DNA-protein complexes was performed with 50µl 50:50 (v/v) Protein G Agarose (Invitrogen) for 2 h at 4 °C, followed by isolation of the DNA. Subsequent Nanog PCR produced 95 bp amplicons. For quantitative ChIP the same procedure was used followed by qRT-PCR analysis (see below). For sequences of ChIP primers see Table 3.

Microarray

Total RNAs extracted from the small intestinal tumors of *Apc^{Min}* and *vil-MACC1/Apc^{Min}* mice were reverse-transcribed and labelled using the Ambion WT expression kit (Ambion) and the GeneChip WT Terminal Labeling Kit (Affymetrix), according to the manufacturer's instructions, and hybridized to GeneChip® Mouse Gene 2.0 ST Arrays (Affymetrix) that target a total of 35,240 transcripts. Arrays were scanned on a Affymetrix Gene Chip Scanner 7G. After data normalization, genes with uniformly low expression were excluded from further analyses. Data were analyzed using GeneSpring GX software (Agilent). Genes with at least 1.5-fold change relative to *Apc^{Min}* control mice were selected.

Tumor sphere formation assay

For the sphere formation assay, single-cell suspensions were seeded in ultra-low attachment 6-well plates (Corning Inc.) in Advanced DMEM/F-12 (Gibco) supplemented with 1x GlutaMAX (Gibco), 1x Pen/Strep (PAA), 10 mM HEPES (Sigma-Aldrich), 1 mM N-Acetylcysteine (Sigma-Aldrich), 1x N-2 Supplement (Gibco), 1x B-27 Supplement (Gibco), 20 ng/ml hFGF basic/FGF2 (Cell Signaling), 50 ng/ml hEGF (Sigma-Aldrich), 10 µM Y-27632 dihydrochloride (Sigma-Aldrich) and 2.5 µg/ml Amphotericin B (Sigma-Aldrich). Per well, 2000 cells were seeded in 2 ml of media. Cells were incubated for 7 days without media change. After incubation, plates were gently shaken to dissociate cell aggregates and directly counted under a phase contrast microscope. For counting, only spheres with a size of >50 µm and a clear round morphology were included.

Statistics

All calculations and statistical analyses were performed with GraphPad Prism version 5.01 (GraphPad Software). For comparison of two groups, unpaired two-tailed Student's *t* test, unpaired two-tailed Student's *t* test with Welch's correction (unequal variances) and Mann Whitney test were used. For correlation analysis, non-parametric Spearman's correlation was used. Kaplan–Meier analysis was used to plot overall survival and differences in curves were analyzed by log-rank test. $P < 0.05$ was considered statistically significant. All results shown represent mean \pm SEM.

Cell culture, Tissue preparation, histology and immunohistochemistry, RNA extraction and qRT-PCR are described in the Supplementary data.

Results

Generation and characterization of vil-MACC1 mice

We generated a transgenic mouse model that expresses MACC1 under the control of the villin promoter (vil-MACC1) (**fig. 1A**). The 12.4-kb mouse villin promoter was previously shown to drive transgene expression predominantly in the epithelial cells of the small intestine (SI) and colon (30). The transgene construct was microinjected into fertilized mouse eggs, and the founder lines were analyzed for their MACC1 transgene expression (**fig. S1A**). All vil-MACC1 lines expressed transgenic MACC1 mRNA and protein in the whole horizontal axis of the intestine (duodenum, jejunum, ileum and colon), but not in other organs such as the liver, lung and kidney (**fig. 1B, 1C** and **fig. S1B**). Transgenic MACC1 mRNA and protein were specifically targeted to the intestinal epithelial cells (IECs) of vil-MACC1 mice (**fig. S1C** and **S1D**). To characterize the transgene expression in the vertical axis of the intestine of these mice, we isolated successive fractions of IECs, from the villus tip (F1) to the crypt (F10). The highest levels of transgenic MACC1 were observed in the F1, with a continuous decrease towards fraction F10 (**fig. 1D** and **1E**). Importantly, we could still detect a significant amount of the transgene in fraction F10. This expression pattern is consistent with the endogenous expression of the villin gene (30) confirming that the MACC1 transgene is expressed in the entire vertical axis, including the cells of the crypts.

To investigate whether MACC1 overexpression in the IECs induced changes in the intestinal epithelium of vil-MACC1 mice, we analyzed haematoxylin and eosin (H&E) sections from the small and large intestine. At 3-months of age, vil-MACC1 mice showed a healthy intestinal mucosa without signs of abnormalities and with normal length (**fig. S2A** and **S2B**). We then aged the vil-MACC1 mice for at least one year (52 – 112 weeks, median 71 weeks) and analyzed the potential tumor development in these animals. We observed small adenomas in the SI of 2 out of 13 (15%) aged vil-MACC1 mice (**fig. S2C**), suggesting that these animals develop tumors at a very low rate and with long latency. The aged vil-MACC1 animals did not show signs of intestinal hyperplasia, as evidenced by the similar intestinal length when compared with littermate WT controls (**fig. S2D**).

Overexpression of MACC1 in the IECs promoted tumor progression in vil-MACC1/Apc^{Min} mice

It has been previously hypothesized that MACC1 induction might occur at the crucial step of transition from the benign (adenoma) to the malignant (carcinoma) phenotype in CRC (9,35). To genetically

address this hypothesis, we crossed the vil-MACC1 transgenic mice with Apc^{Min} mice (36) to generate vil-MACC1/ Apc^{Min} animals. The Apc^{Min} mice are a classical model for intestinal tumorigenesis, which develop an average of 30 – 40 tumors, predominantly in the SI and histologically classified as benign adenomas (32,33). The vil-MACC1/ Apc^{Min} mice expressed transgenic MACC1 mRNA in the small and large intestine at a similar level as vil-MACC1 mice. They also expressed the transgenic mRNA in the intestinal tumors, but not in the liver (**fig. S3A**). Immunofluorescence staining revealed MACC1 transgenic protein in the epithelial cells of the SI and colon, as well as in tumor tissues of vil-MACC1/ Apc^{Min} mice (**fig. S3B**). We evaluated the number and size of tumors formed in the SI and colon of vil-MACC1/ Apc^{Min} and their Apc^{Min} littermate controls. At 6 months of age (25 ± 2 weeks), vil-MACC1/ Apc^{Min} mice had a significantly higher number of tumors in the whole intestine as compared with Apc^{Min} controls (average of 73.57 ± 6.181 vs. 46.36 ± 6.358 , respectively; $P = 0.0056$; **fig. 2A**). A similar tendency was already observed at 4 months of age (17 ± 2 weeks), but without statistical significance (**fig. S4A**). The majority of the tumors were formed in the SI of both mouse models. Interestingly, we observed not only an increase in the total number but also in the size of those tumors in the vil-MACC1/ Apc^{Min} mice (**fig. 2B**), as illustrated in **fig. 2C**. No difference was observed between Apc^{Min} and vil-MACC1/ Apc^{Min} mice regarding the small (≤ 1 mm in diameter; $P = 0.2895$) tumors. The difference became evident for the intermediate-sized tumors (2 mm in diameter; $P = 0.0448$), and was very clear for large tumors (≥ 3 mm in diameter; $P = 0.0024$). Consistent with the reported increased tumor burden in vil-MACC1/ Apc^{Min} mice, we observed a significant decrease in their overall survival as compared with Apc^{Min} littermates (median survival was 23 and 26 weeks, respectively; $P = 0.03$; **fig. 2D**).

A detailed histological analysis of the tumors from both groups of animals revealed that the vil-MACC1/ Apc^{Min} mice developed bigger tumors, which were highly proliferative as evidenced by the Ki-67 staining (**fig. 3A-C** and **3L-N**). The pathological analysis demonstrated that the tumors from the vil-MACC1/ Apc^{Min} mice had a more invasive phenotype, with destruction of the basement membrane and invasion of epithelial cells into the lamina propria (**fig. 3D, 3G** and **3I**). Some of those tumors showed the presence of back-to-back glands (**fig. 3E**) and budding, together with nuclear β -catenin accumulation (**fig. 3F** and **3K**).

It has been previously described that Apc^{Min} mice develop splenomegaly (39). Some studies reported a correlation between the severity of the tumorigenesis and the spleen size (39,40). Consistently, we observed a very strong positive correlation between the spleen size and number of tumors in the vil-

MACC1/Apc^{Min} and Apc^{Min} mice (**fig. S4B**). We confirmed the development of splenomegaly in the Apc^{Min} mice, a phenotype that was even more prominent in the vil-MACC1/Apc^{Min} animals (**fig. S4C** and **S4D**).

Altogether, our results constitute robust evidence for the presence of an accelerated adenoma-carcinoma sequence in the vil-MACC1/Apc^{Min} mice, supporting the role of MACC1 on tumor progression in vivo.

The SI tumors of vil-MACC1/Apc^{Min} display increased Wnt and pluripotency signaling

To further investigate the molecular mechanism underlying MACC1-induced tumor progression, we performed a genome-wide mRNA expression analysis (Affymetrix microarrays) comparing the SI tumors from vil-MACC1/Apc^{Min} and Apc^{Min} mice. A total of 766 probes representing 760 genes were differentially expressed in the two groups (FC > 1.5; P = 0.05) (**fig. 4A**). We then performed a pathway analysis to find relevant pathways associated with the tumors of vil-MACC1/Apc^{Min} mice. Prominently, we found “Wnt signaling and pluripotency” pathway with members significantly enriched in the list of upregulated genes in those mice (**fig. S5**). From the identified genes belonging to the “Wnt signaling and pluripotency” pathway, the majority were nucleus-associated, suggesting a potential increase in the transcriptional activity of this pathway. To validate these findings, we analyzed the mRNA levels of some relevant genes in the SI tumors of both groups of mice by qRT-PCR. We found several Wnt related genes upregulated in the tumors of vil-MACC1/Apc^{Min} mice compared with Apc^{Min} controls. Among those were different extracellular matrix modulators, including the urokinase plasminogen activator (PLAU), matrix metalloproteinase 7 (MMP7) and matrix metalloproteinase 9 (MMP9). Additionally, we found the lymphoid enhancer-binding factor 1 (LEF1), the vascular endothelial growth factor A (VEGFA) and the tumor necrosis factor receptor superfamily, member 19 (TNFRSF19; also known as TROY) to be upregulated in the SI tumors of vil-MACC1/Apc^{Min} mice (**fig. 4B**). TROY is a tissue-specific Wnt target gene, which is produced specifically by fast-cycling intestinal stem cells (41). This observation prompted us to analyze other stem cell related genes which are also Wnt target genes. We found the leucine-rich repeat-containing G-protein coupled receptor 5 (Lgr5) and CD44 to be expressed at similar levels in the tumors of both mouse groups. However, we observed a prominent upregulation of the pluripotency markers octamer-binding transcription factor 4 (Oct4; also known as POU5F1 (POU domain, class 5, transcription factor 1)) and Nanog in the SI tumors of vil-MACC1/Apc^{Min} mice, compared with Apc^{Min} controls (**fig. 4C**). These results suggest that an activation

of the pluripotency signaling might, at least in part, be responsible for the MACC1-induced tumor progression observed in the *vil-MACC1/Apc^{Min}* mice.

MACC1 regulates the pluripotency markers Oct4 and Nanog

We selected a panel of CRC cell lines with different endogenous levels of MACC1 and manipulated MACC1 levels through its ectopic overexpression or knockdown (**fig. 5A**). Strikingly, we found that upon MACC1 overexpression in SW480 and Caco-2 cells, the mRNA levels of Oct4 and Nanog were significantly increased. Conversely, upon MACC1 knockdown in SW620 and Caco-2 cells, the mRNA levels of Oct4 and Nanog were significantly decreased (**fig. 5B** and **5D**). While we were not successful to assess the protein levels of Nanog in these cells, the levels of Oct4 show a corresponding trend in all manipulated cell lines (**fig. 5C**). In order to elucidate how MACC1 might regulate the transcription of Oct4 and Nanog, we performed chromatin immunoprecipitation experiments. While no indications for a binding of MACC1 to the Oct4 gene promoter could be found, we did confirm a physical binding of MACC1 to the gene promoter of Nanog in MACC1-overexpressing CRC cells (**fig. 5E**). This gives evidence to a model where MACC1 binds to the Nanog promoter, thereby inducing the expression of Nanog which can in turn trigger the upregulation of Oct4 and confer other stem-like traits (**fig. 5F**) (42). We performed a tumor sphere formation assay as a functional read-out for stemness in SW480/MACC1 CRC cells. Cells were grown in serum-free, non-adherent conditions favoring survival and proliferation of stem/progenitor cells. Strikingly, the number and size of spheres formed after one week was significantly higher in the SW480/MACC1 cells, compared with SW480/e.v. control cells (**fig. 5F**).

Furthermore, we analyzed the mRNA levels of Oct4 and Nanog in a cohort of 60 tumors from CRC patients and correlated them with MACC1 expression. These patients were diagnosed without distant metastases (stages 1, 2, and 3) at the time point of surgery, had no familial history of colon cancer, no tumor of the same or a second entity, were previously untreated and underwent surgical R0 resection. We found a very significant positive correlation between Oct4 and MACC1 mRNA levels ($r = 0.7005$; $P > 0.0001$) as well as between Nanog and MACC1 ($r = 0.6808$; $P > 0.0002$) (**fig. 6A** and **6C**). Consistently, we observed significantly higher levels of Oct4 and Nanog mRNA in the group of patients with high MACC1 expression (**fig. 6B** and **6D**). Further, correlation of Oct4 and Nanog expression levels was also of statistical significance ($P < 0.0001$) (**fig. 6E**).

Discussion

The prognostic value of MACC1 for tumor progression and metastasis has been established in many different solid cancers, including CRC (10). However, it remains unclear whether MACC1 alone has the potential to induce neoplastic transformation in the normal intestinal epithelium. Here we report the generation of the first MACC1 genetically engineered mouse models vil-MACC1 and vil-MACC1/Apc^{Min}. MACC1 overexpression in an Apc-mutated background significantly exacerbates tumor formation and progression by increased expression of the pluripotency genes Oct4 and Nanog. These observations corroborate our initial hypothesis and allocate MACC1 to the transition of benign adenoma to malignant carcinoma in the adenoma-carcinoma model of CRC development. Several lines of evidence suggest that MACC1 regulates the pluripotency markers and Wnt target genes Oct4 and Nanog: the SI tumors of vil-MACC1/Apc^{Min} mice have significantly higher levels of Oct4 and Nanog than those of Apc^{Min} controls; manipulation of MACC1 levels in a panel of CRC cell lines induce a concomitant change in the expression levels of Oct4 and Nanog; the MACC1 mRNA levels strongly correlate with those of Oct4 and Nanog in a cohort of 60 tumors from CRC patients. Oct4 and Nanog are expressed mainly in embryonic stem cells and only in very low levels in normal adult tissues (42–44). However, an increasing number of studies demonstrate that both Oct4 and Nanog are aberrantly overexpressed in different types of cancer, contributing to the stem-cell phenotype of tumor cells (45,46). Consistently, it has been demonstrated that overexpression of Oct4 and Nanog in epithelial cells promotes tumorigenesis and metastasis (47,48). Furthermore, elevated expression of Nanog predicts poor prognosis in hepatocellular carcinoma and CRC (46,49). Therefore, one can hypothesize that the MACC1-induced tumor progression is mediated by an increased level of the pluripotency markers Oct4 and Nanog. Of note, similarly to what has been reported for Oct4 and Nanog, the levels of MACC1 are very low in normal adult tissues and aberrantly increased in tumor samples (7). Whether MACC1 is expressed during embryogenesis and plays a role in organ formation and/or development remains unclear. However, initial evidence demonstrated that MACC1 might be involved in the development of the craniofacial skeleton of zebrafish (50).

In conclusion, we report for the first time the generation and characterization of MACC1 genetically engineered mouse models, which provided strong evidence for the role of MACC1 in intestinal tumor progression. Furthermore, these novel transgenic mouse models constitute an important tool to unravel novel molecular mechanisms underlying MACC1-associated phenotypes. Thereby, we

demonstrated that MACC1 induces the master regulators of pluripotency, Nanog and Oct4. We deduce that MACC1's tumor and metastasis promoting effect might in part be mediated by its role in stem cell signaling via the newly discovered MACC1/Nanog/Oct4 axis. Additional experiments will further elucidate the function of MACC1 in the context of cancer stem cells. The interconnection of MACC1 with major regulators of pluripotency might offer novel options for therapeutic intervention strategies to restrict tumor progression.

Acknowledgements

We are thankful to Sanchita Ghosh, Gonçalo Regalo, Gabriele Born, Katerina Vlantis and Gabriele Hörmannsperger for technical assistance. We are also obliged to Deborah Gumucio for providing the p12.4kbVillin- Δ ATG vector. We thank our lab members Dennis Kobelt, Mathias Dahlmann, Fabian Zincke and Jessica Pahle for contributing in the revision process.

References

1. Ferlay J, Shin H-R, Bray F, Forman D, Mathers C, Parkin DM. Estimates of worldwide burden of cancer in 2008: GLOBOCAN 2008. *Int J Cancer*. 2010;127:2893–917.
2. Fearon ER, Vogelstein B. A genetic model for colorectal tumorigenesis. *Cell*. 1990;61:759–67.
3. Kinzler KW, Vogelstein B. Lessons from Hereditary Colorectal Cancer. *Cell*. 1996;87:159–70.
4. Fodde R, Smits R, Clevers H. APC, signal transduction and genetic instability in colorectal cancer. *Nat Rev Cancer*. 2001;1:55–67.
5. Markowitz SD, Bertagnolli MM. Molecular origins of cancer: Molecular basis of colorectal cancer. *N Engl J Med*. 2009;361:2449–60.
6. Clevers H, Nusse R. Wnt/ β -catenin signaling and disease. *Cell*. 2012;149:1192–205.
7. Stein U, Walther W, Arlt F, Schwabe H, Smith J, Fichtner I, et al. MACC1, a newly identified key regulator of HGF-MET signaling, predicts colon cancer metastasis. *Nat Med*. 2009;15:59–67.
8. Zhen T, Dai S, Li H, Yang Y, Kang L, Shi H, et al. MACC1 promotes carcinogenesis of colorectal cancer via β -catenin signaling pathway. *Oncotarget*.
9. Arlt F, Stein U. Colon cancer metastasis: MACC1 and Met as metastatic pacemakers. *Int J Biochem Cell Biol*. 2009;41:2356–9.
10. Stein U. MACC1 - a novel target for solid cancers. *Expert Opin Ther Targets*. 2013;17:1039–52.
11. Zheng Z, Gao S, Yang Z, Xie H, Zhang C, Lin B, et al. Single nucleotide polymorphisms in the metastasis-associated in colon cancer-1 gene predict the recurrence of hepatocellular carcinoma after transplantation. *Int J Med Sci*. 2014;11:142–50.
12. Gao S, Lin B-Y, Yang Z, Zheng Z-Y, Liu Z-K, Wu L-M, et al. Role of overexpression of MACC1 and/or FAK in predicting prognosis of hepatocellular carcinoma after liver transplantation. *Int J Med Sci*. 2014;11:268–75.
13. Xie C, Wu J, Yun J, Lai J, Yuan Y, Gao Z, et al. MACC1 as a prognostic biomarker for early-stage and AFP-normal hepatocellular carcinoma. *PLoS One*. 2013;8:e64235.
14. Ji D, Lu Z-T, Li Y-Q, Liang Z-Y, Zhang P-F, Li C, et al. MACC1 expression correlates with PFKFB2 and survival in hepatocellular carcinoma. *Asian Pac J Cancer Prev*. 2014;15:999–1003.
15. Yang Y-P, Qu J-H, Chang X-J, Lu Y-Y, Bai W-L, Dong Z, et al. High intratumoral metastasis-associated in colon cancer-1 expression predicts poor outcomes of cryoablation therapy for advanced hepatocellular carcinoma. *J Transl Med*. 2013;11:41.
16. Gao J, Ding F, Liu Q, Yao Y. Knockdown of MACC1 expression suppressed hepatocellular carcinoma cell migration and invasion and inhibited expression of MMP2 and MMP9. *Mol Cell Biochem*. 2012;
17. Qu J-H, Chang X-J, Lu Y-Y, Bai W-L, Chen Y, Zhou L, et al. Overexpression of metastasis-associated in colon cancer 1 predicts a poor outcome of hepatitis B virus-related hepatocellular carcinoma. *World J Gastroenterol*. 2012;18:2995–3003.

18. Qiu J, Huang P, Liu Q, Hong J, Li B, Lu C, et al. Identification of MACC1 as a novel prognostic marker in hepatocellular carcinoma. *J Transl Med.* 2011;9:166.
19. Shirahata A, Fan W, Sakuraba K, Yokomizo K, Goto T, Mizukami H, et al. MACC 1 as a marker for vascular invasive hepatocellular carcinoma. *Anticancer Res.* 2011;31:777–80.
20. Wang L, Wu Y, Lin L, Liu P, Huang H, Liao W, et al. MACC1 upregulation predicts a poor prognosis of gastric cancer, and promotes tumor cell proliferation and invasion. *Int J Cancer.* 2013;
21. Guo T, Yang J, Yao J, Zhang Y, Da M, Duan Y. Expression of MACC1 and c-Met in human gastric cancer and its clinical significance. *Cancer Cell Int.* 2013;13:121.
22. Wang J, Hong Q, Hu C, Fang Y, Wang Y. [Significance of MACC1 protein expression in esophageal carcinoma]. *Zhonghua Yi Xue Za Zhi.* 2013;93:2584–6.
23. Zhu M, Xu Y, Mao X, Gao Y, Shao L, Yan F. Overexpression of Metastasis-Associated in Colon Cancer-1 Associated with Poor Prognosis in Patients with Esophageal Cancer. *Pathol Oncol Res.* 2013;
24. Chen X-P, Ren X-P, Lan J-Y, Chen Y-G, Shen Z-J. Analysis of HGF, MACC1, C-met and apoptosis-related genes in cervical carcinoma mice. *Mol Biol Rep.* 2014;
25. Chai H, Yang Y. Effects of MACC1 siRNA on biological behaviors of HeLa. *Arch Gynecol Obstet.* 2013;
26. Wang Z, Li Z, Wu C, Wang Y, Xia Y, Chen L, et al. MACC1 overexpression predicts a poor prognosis for non-small cell lung cancer. *Med Oncol.* 2014;31:790.
27. Shimokawa H, Uramoto H, Onitsuka T, Chundong G, Hanagiri T, Oyama T, et al. Overexpression of MACC1 mRNA in lung adenocarcinoma is associated with postoperative recurrence. *J Thorac Cardiovasc Surg.* 2011;141:895–8.
28. Chundong G, Uramoto H, Onitsuka T, Shimokawa H, Iwanami T, Nakagawa M, et al. Molecular diagnosis of MACC1 status in lung adenocarcinoma by immunohistochemical analysis. *Anticancer Res.* 2011;31:1141–5.
29. Merlos-Suárez A, Barriga FM, Jung P, Iglesias M, Céspedes MV, Rossell D, et al. The intestinal stem cell signature identifies colorectal cancer stem cells and predicts disease relapse. *Cell Stem Cell.* 2011;8:511–24.
30. Madison BB, Dunbar L, Qiao XT, Braunstein K, Braunstein E, Gumucio DL. Cis elements of the villin gene control expression in restricted domains of the vertical (crypt) and horizontal (duodenum, cecum) axes of the intestine. *J Biol Chem.* 2002;277:33275–83.
31. Stein U, Walther W, Arlt F, Schwabe H, Smith J, Fichtner I, et al. MACC1, a newly identified key regulator of HGF-MET signaling, predicts colon cancer metastasis. *Nat Med.* 2009;15:59–67.
32. Vlantis K, Wullaert A, Sasaki Y, Schmidt-Supprian M, Rajewsky K, Roskams T, et al. Constitutive IKK2 activation in intestinal epithelial cells induces intestinal tumors in mice. *J Clin Invest.* 2011;121:2781–93.
33. Ferraris RP, Villenas SA, Diamond J. Regulation of brush-border enzyme activities and enterocyte migration rates in mouse small intestine. *Am J Physiol Gastrointest Liver Physiol.* 1992;262:G1047–59.

34. Stein U, Arlt F, Walther W, Smith J, Waldman T, Harris ED, et al. The metastasis-associated gene S100A4 is a novel target of beta-catenin/T-cell factor signaling in colon cancer. *Gastroenterology*. 2006;131:1486–500.
35. Ren B, Zakharov V, Yang Q, McMahon L, Yu J, Cao W. MACC1 is related to colorectal cancer initiation and early-stage invasive growth. *Am J Clin Pathol*. 2013;140:701–7.
36. Moser AR, Pitot HC, Dove WF. A dominant mutation that predisposes to multiple intestinal neoplasia in the mouse. *Science*. 1990;247:322–4.
37. Boivin GP, Washington K, Yang K, Ward JM, Pretlow TP, Russell R, et al. Pathology of mouse models of intestinal cancer: Consensus report and recommendations. *Gastroenterology*. 2003;124:762–77.
38. Taketo MM, Edelmann W. Mouse models of colon cancer. *Gastroenterology*. 2009;136:780–98.
39. Zeineldin M, Neufeld KL. Understanding Phenotypic Variation in Rodent Models with Germline Apc Mutations. *Cancer Res*. 2013;73:2389–99.
40. Asfaha S, Dubeykovskiy AN, Tomita H, Yang X, Stokes S, Shibata W, et al. Mice that express human interleukin-8 have increased mobilization of immature myeloid cells, which exacerbates inflammation and accelerates colon carcinogenesis. *Gastroenterology*. 2013;144:155–66.
41. Fafilek B, Krausova M, Vojtechova M, Pospichalova V, Tumova L, Sloncova E, et al. Troy, a tumor necrosis factor receptor family member, interacts with lgr5 to inhibit wnt signaling in intestinal stem cells. *Gastroenterology*. 2013;144:381–91.
42. Boyer LA, Lee TI, Cole MF, Johnstone SE, Levine SS, Zucker JP, et al. Core transcriptional regulatory circuitry in human embryonic stem cells. *Cell*. 2005;122:947–56.
43. Chambers I, Silva J, Colby D, Nichols J, Nijmeijer B, Robertson M, et al. Nanog safeguards pluripotency and mediates germline development. *Nature*. Nature Publishing Group; 2007;450:1230–4.
44. Niwa H, Miyazaki J, Smith AG. Quantitative expression of Oct-3/4 defines differentiation, dedifferentiation or self-renewal of ES cells. *Nat Genet*. 2000;24:372–6.
45. Noh KH, Kim BW, Song K-H, Cho H, Lee Y-H, Kim JH, et al. Nanog signaling in cancer promotes stem-like phenotype and immune evasion. *J Clin Invest*. American Society for Clinical Investigation; 2012;122:4077–93.
46. Shan J, Shen J, Liu L, Xia F, Xu C, Duan G, et al. Nanog regulates self-renewal of cancer stem cells through the insulin-like growth factor pathway in human hepatocellular carcinoma. *Hepatology*. 2012;56:1004–14.
47. Hochedlinger K, Yamada Y, Beard C, Jaenisch R. Ectopic expression of Oct-4 blocks progenitor-cell differentiation and causes dysplasia in epithelial tissues. *Cell*. 2005;121:465–77.
48. Lu X, Mazur SJ, Lin T, Appella E, Xu Y. The pluripotency factor nanog promotes breast cancer tumorigenesis and metastasis. *Oncogene*. Macmillan Publishers Limited; 2014;33:2655–64.
49. Meng H-M, Zheng P, Wang X-Y, Liu C, Sui H-M, Wu S-J, et al. Overexpression of nanog predicts tumor progression and poor prognosis in colorectal cancer. *Cancer Biol Ther*. 2010;9.
50. Melvin VS, Feng W, Hernandez-Lagunas L, Artinger KB, Williams T. A morpholino-based screen to identify novel genes involved in craniofacial morphogenesis. *Dev Dyn*. 2013;

Figure Legends

Figure 1. Expression of the MACC1 transgene in vil-MACC1 mice. **(A)** Diagram of the MACC1 transgene. **(B)** qRT-PCR analysis revealed transgenic MACC1 mRNA expression in the duodenum, jejunum, ileum and colon, but not in the liver, lung and kidney of 4 vil-MACC1 transgenic lines (T8892, T9757, T9760 and T9765). Data represent mean \pm SEM ($n \geq 4$, per genotype). **(C)** Immunofluorescent staining with an anti-MACC1 antibody shows expression of MACC1 in the epithelial cells of the duodenum, jejunum, ileum and colon, but not in the liver of vil-MACC1 mice. The depicted images are representative of WT (lower row) and vil-MACC1 (line T9757, upper row) mice with MACC1 stained in red (Cy3) and the nuclei stained in blue (DAPI). Scale bars: 100 μ m. Transgenic MACC1 mRNA **(D)** and protein **(E)** were detected along the entire vertical axis (from villus tip (F1) to crypt (F10)) of the SI of vil-MACC1 transgenic mice (line T9757). mRNA data represent mean \pm SEM ($n = 2$). A representative blot of 2 independent experiments is shown.

Figure 2. MACC1 overexpression increases tumor burden and reduces survival of vil-MACC1/Apc^{Min} mice. **(A)** The vil-MACC1/Apc^{Min} mice showed a significant increase in the total number of intestinal tumors. **(B)** The most prominent increase was observed for the bigger tumors (diameter ≥ 3 mm) in the SI. Quantification was performed by two independent researchers for vil-MACC1/Apc^{Min} ($n = 14$) and Apc^{Min} ($n = 11$) control mice at 25 ± 2 weeks of age. P values were calculated using unpaired two-tailed Student's t test with Welch's correction. **(C)** Gross pictures and H&E stainings on representative sections of the ileum of three vil-MACC1/Apc^{Min} and three Apc^{Min} mice show the increase in the number and size of tumors in the former as compared to the latter. Scale bars: 2 mm. **(D)** Kaplan–Meier survival analysis revealed that vil-MACC1/Apc^{Min} mice ($n = 38$) have a significantly shorter survival as compared with Apc^{Min} control mice ($n = 32$). The end point for survival was defined as the time of death or the time at which the mice were sacrificed due to severe tumor-related disease. Statistics were evaluated by the P log-rank test.

Figure 3. MACC1 overexpression induces tumor progression *in vivo*.

(A,B,C) The presence of bigger tumors in the SI of vil-MACC1/Apc^{Min} (B,C) mice compared to Apc^{Min} mice (A) is evident in a more detailed analysis of H&E stainings.

(D,E) Histological analysis of SI sections from vil-MACC1/ApcMin mice revealed the presence of high grade adenomas with stromal invasion (solid arrows), the presence of dissociated invasive cells (arrowhead), intraepithelial budding (arrows) (D) and back-to-back glands (arrowheads) (E).

(F) High grade adenomas with tumor budding (arrowheads) were also present in the colon of vil-MACC1/ApcMin mice, as revealed by the H&E staining.

(G) The presence of stromal invasion in the SI tumors of vil-MACC1/ApcMin mice can also be observed in the Masson-Goldner staining (arrowheads).

(H,I) Immunostaining with Collagen IV revealed the destruction of the basal membrane in the vil-MACC1/ApcMin mice (I) (arrowheads) compared to ApcMin mice (H).

(J,K) A strong nuclear accumulation of β -catenin can be observed in the SI tumors of vil-MACC1/ApcMin mice (K) as well as the presence of tumor budding (arrowheads), compared to ApcMin mice (J).

(L,M,N) Immunostaining for Ki-67 revealed strong proliferation of the epithelial cells in the SI tumors of both vil-MACC1/ApcMin (M,N) and ApcMin mice (L). Scale bars: 100 μ m.

Scale bars: 100 μ m (A-G, L-N), 25 μ m (H-K).

Figure 4. Tumors of vil-MACC1/Apc^{Min} mice display an increased activation of Wnt and pluripotency signaling. (A) Microarray analysis comparing the SI tumors of vil-MACC1/Apc^{Min} and Apc^{Min} mice identified 766 probes representing 760 genes differentially expressed in the two groups (FC>1.5; P<0.05). (B) The overexpression of several Wnt-related genes in the SI tumors of vil-MACC1/Apc^{Min} mice was validated by qRT-PCR. Data represent mean \pm SEM (n \geq 4, per genotype). (C) The pluripotency markers Oct4 and Nanog, but not Lgr5 and CD44, were overexpressed in the SI tumors of vil-MACC1/Apc^{Min} mice, as revealed by qRT-PCR. Data represent mean \pm SEM (n \geq 9, per genotype). P values were calculated using unpaired two-tailed Student's *t* test with Welch's correction.

Figure 5. MACC1 regulates the pluripotency markers Oct4 and Nanog. (A) MACC1 mRNA expression in CRC cells following its ectopic overexpression or knockdown. (B) Upon ectopic overexpression of MACC1 in the CRC cells SW480 and Caco-2, an increase in the Oct4 mRNA expression levels was detected by qRT-PCR. Consistently, knockdown of MACC1 in Caco-2 and SW620 cells resulted in decreased levels of Oct4. Data represent mean \pm SEM (n = 3). P values were calculated using

unpaired two-tailed Student's *t* test. (C) Western blotting analyses in the same panel of cell lines revealed a correlation of Oct4 protein levels. (D) The mRNA expression levels of Nanog showed an analogous trend compared to Oct4 across the panel of CRC cells. Data represent mean \pm SEM (n = 3). *P* values were calculated using unpaired two-tailed Student's *t* test. (E) CHIP for binding of MACC1 to the Nanog promoter region -173 to -79. Virtually no Nanog product was detectable in the SW480/e.v. cells and IgG controls. (F) Proposed model for a MACC1-mediated tumor- and metastasis promoting effect via Nanog. (G) In a tumor sphere formation assay, SW480/MACC1 CRC cells displayed a significantly higher number of spheres, which were significantly bigger as compared to SW480/e.v. control cells. Data represent mean \pm SEM (n = 6). *P* value was calculated using unpaired two-tailed Student's *t* test. Scale bars: 100 μ m.

Figure 6. MACC1 expression strongly correlates with Oct4 and Nanog expression in CRC patients. (A)

A strong and statistically significant positive correlation was found between the mRNA levels of Oct4 and MACC1 in the tumors of 60 CRC patients. (B) Patients with high MACC1 mRNA expression had a significantly higher expression of Oct4 mRNA, as determined by qRT-PCR. (C) Correlation analysis revealed that the mRNA levels of MACC1 and Nanog are also positively correlated. (D) The levels of Nanog mRNA were significantly higher in patients with high MACC1 mRNA expression. (E) A strong positive correlation was also found for Oct4 and Nanog mRNA levels in the 60 CRC patients. MACC1, Oct4 and Nanog mRNA levels were determined by qRT-PCR, normalized to the house-keeping gene hGAPDH and calculated as fold of the calibrator. Correlation analysis was performed with non-parametric Spearman's correlation. Classification of patients as low and high MACC1 expressers was performed using MACC1 median expression as cut-off. *P* values in (B) and (D) were calculated using two-tailed Mann Whitney test.

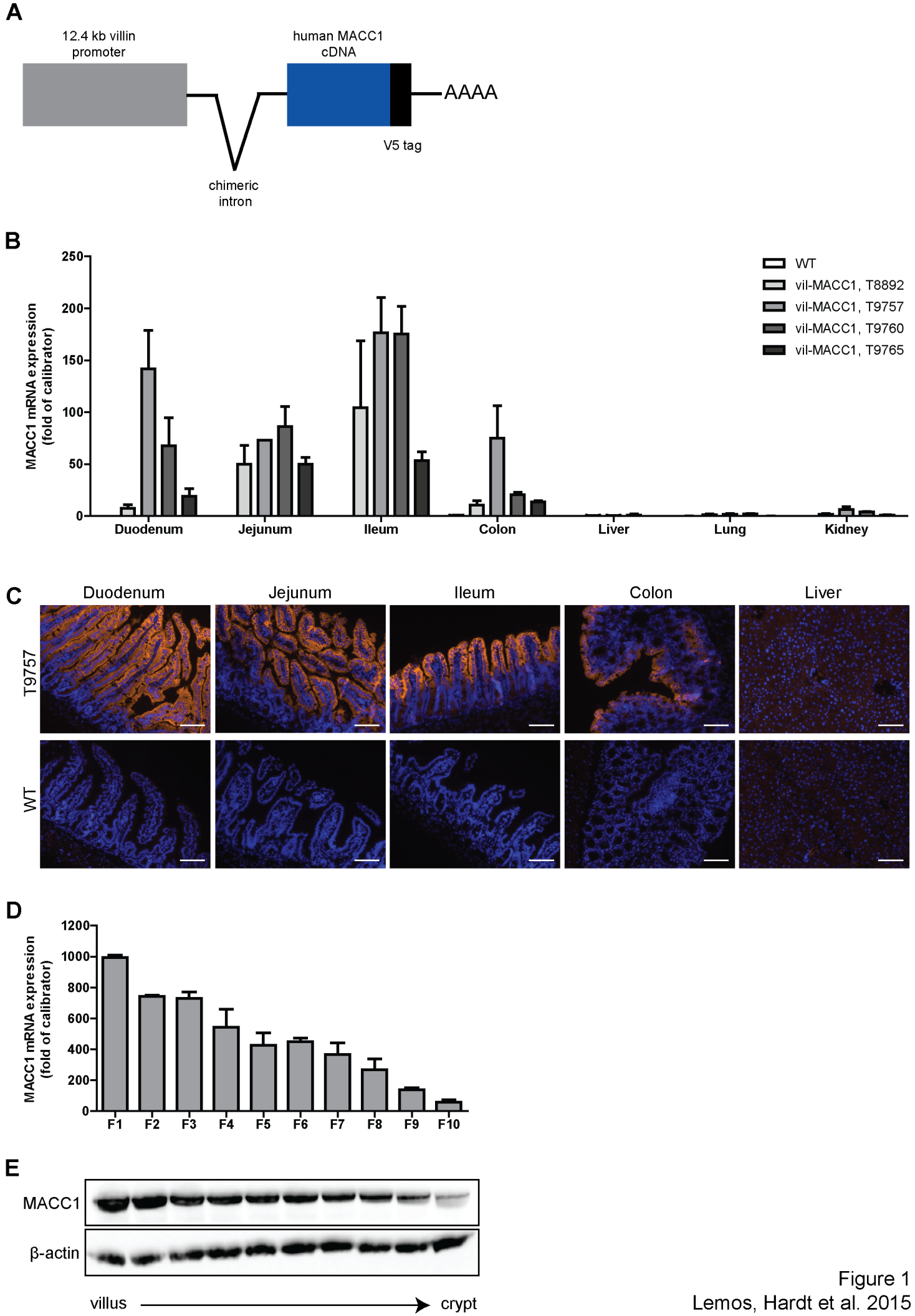


Figure 1
Lemos, Hardt et al. 2015

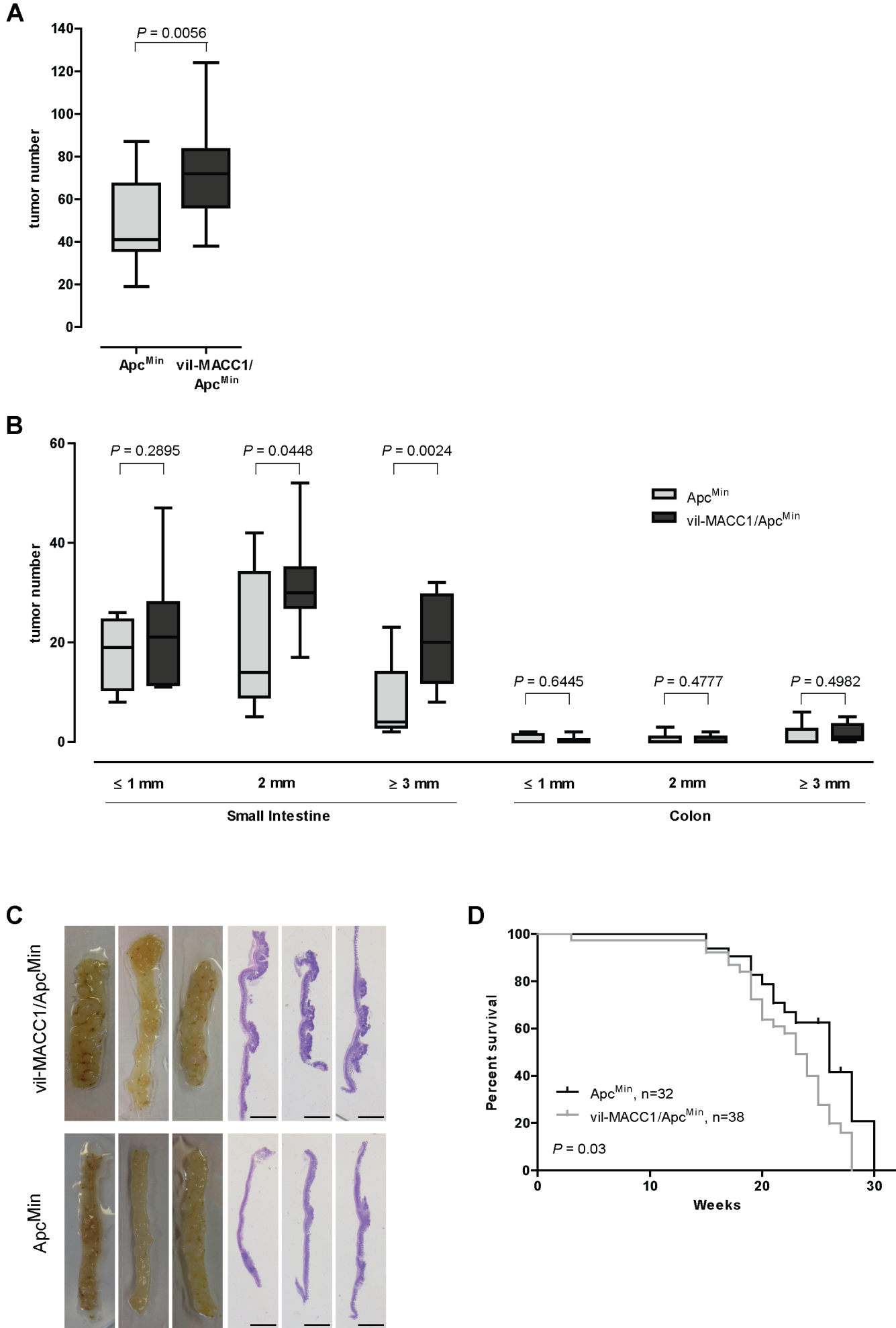


Figure 2
Lemos, Hardt et al. 2015

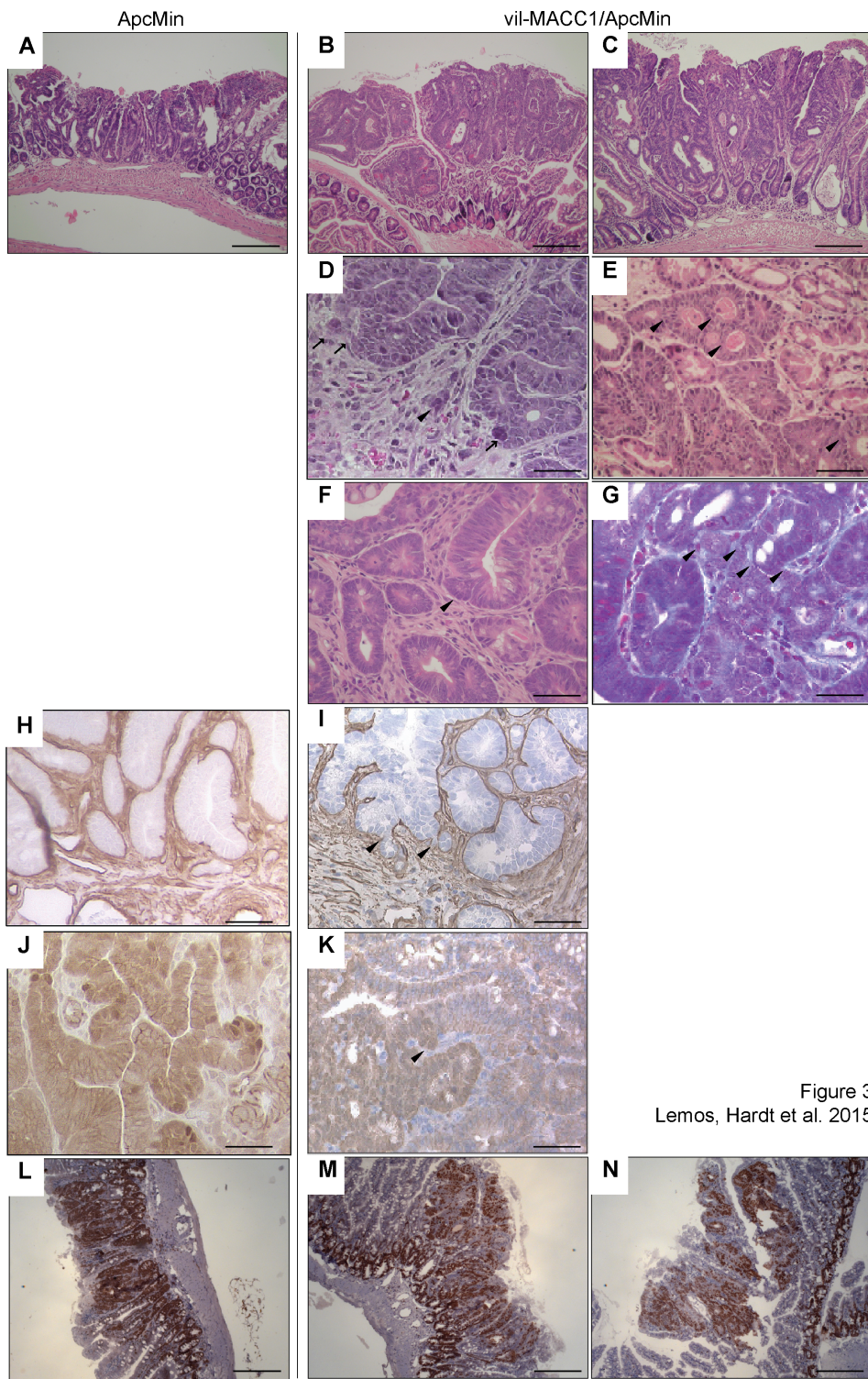


Figure 3
Lemos, Hardt et al. 2015

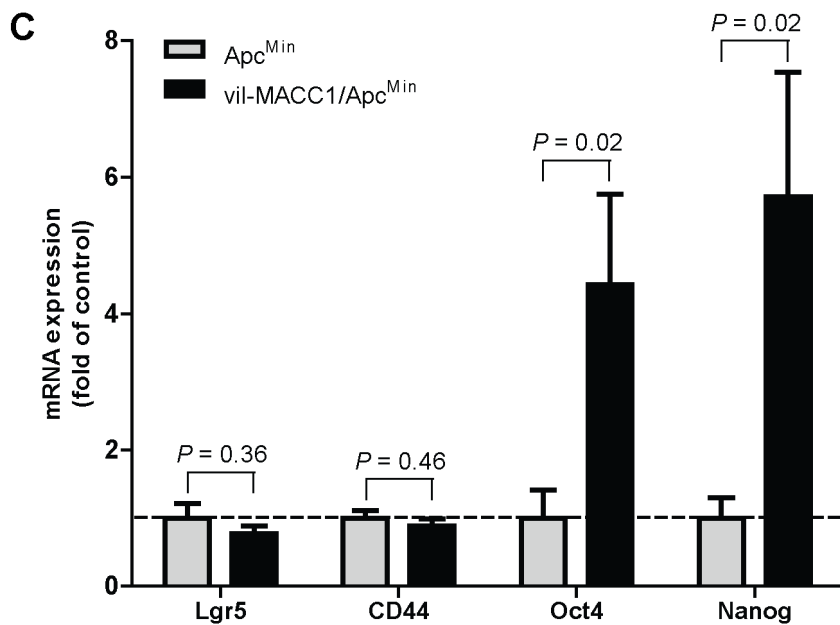
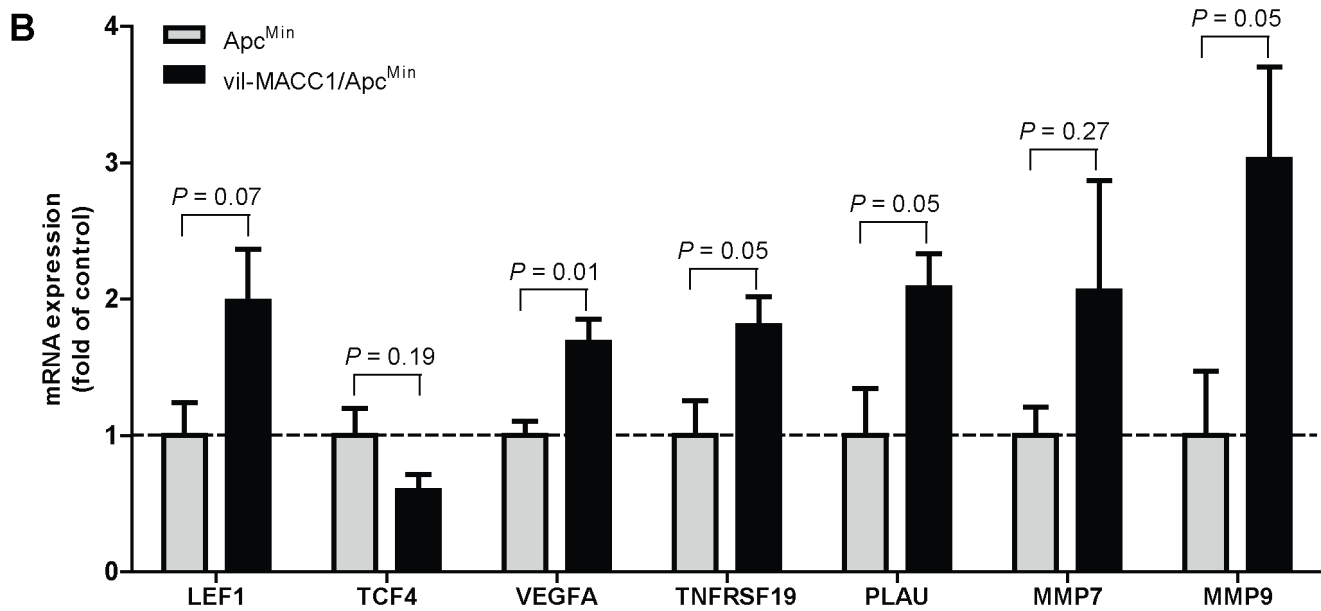
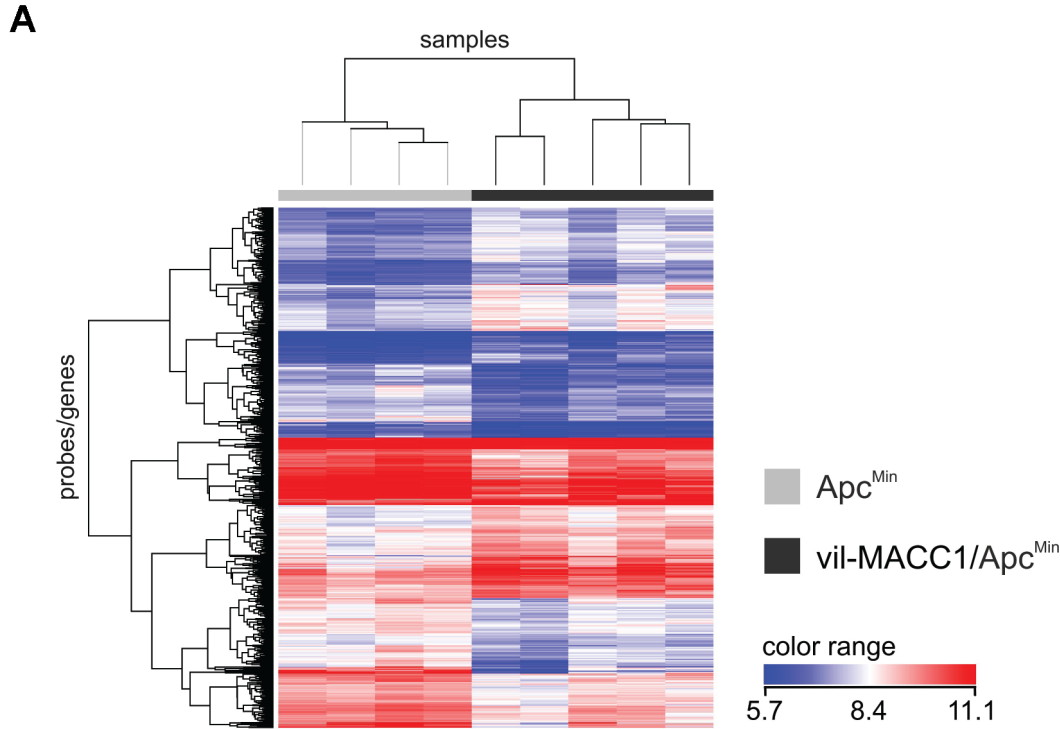


Figure 4
Lemos, Hardt et al. 2015

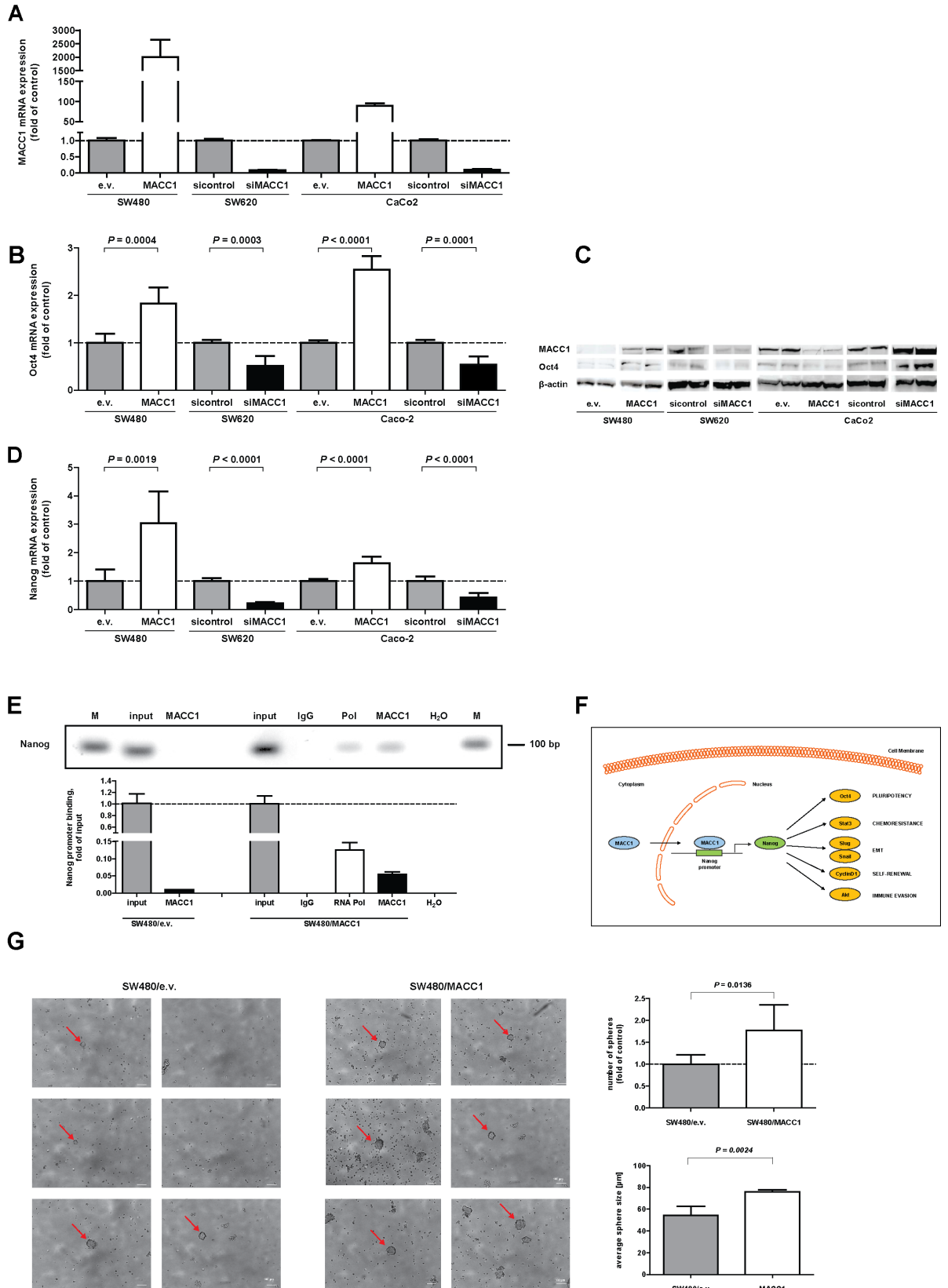


Figure 5
Lemos, Hardt et al. 2015

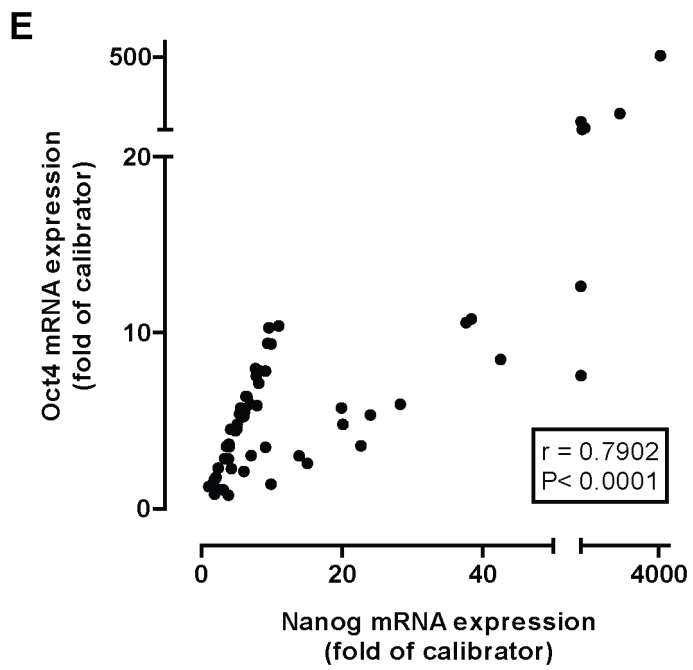
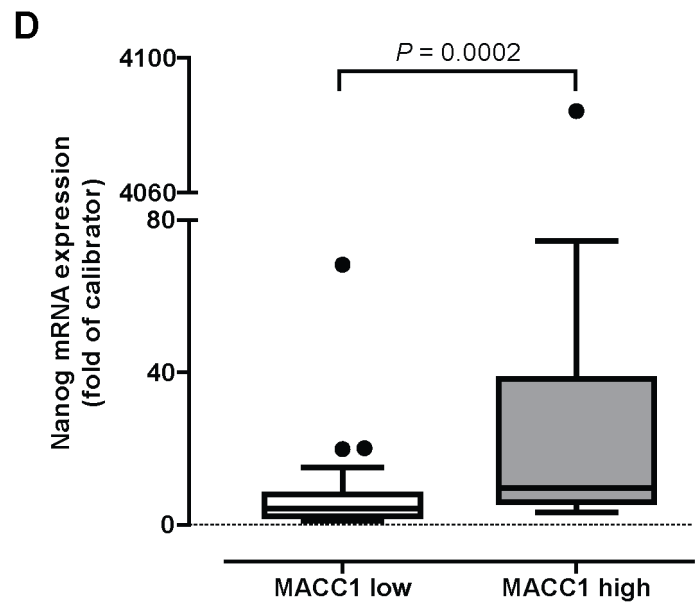
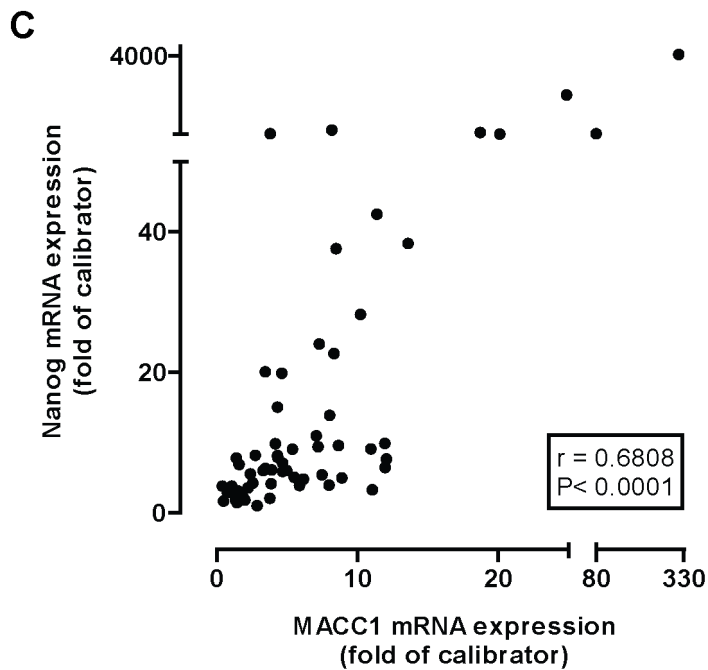
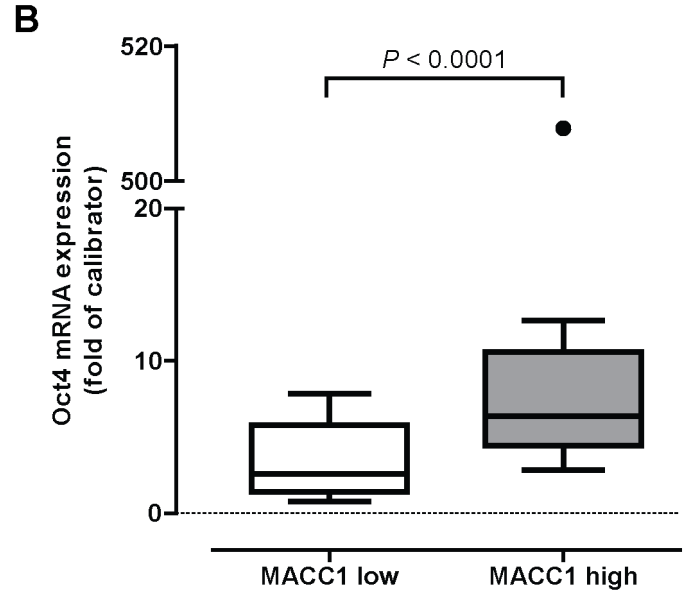
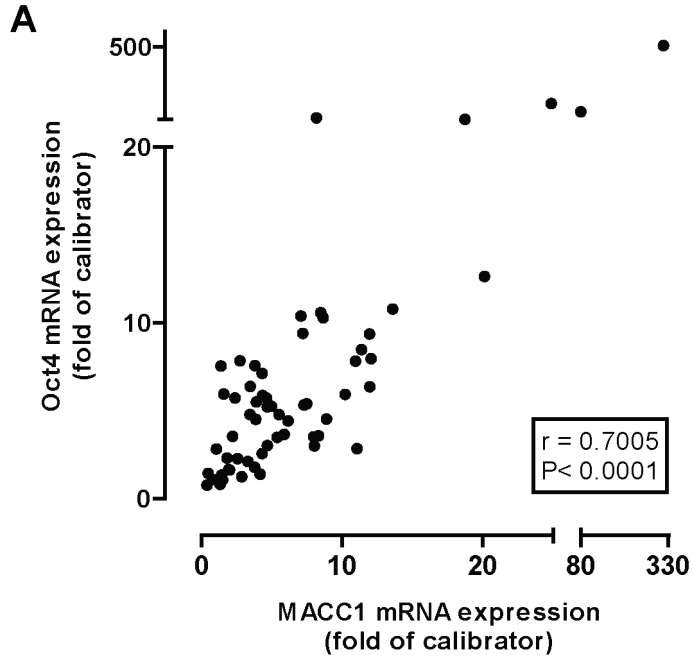


Figure 6
Lemos, Hardt et al. 2015

Supplementary data

Materials and Methods

Cell culture

Human colorectal cancer cell lines HCT116, SW620 and SW480 were obtained from ATCC. Caco-2 cells were generously provided by Dr. Iduna Fichtner (Max-Delbrück-Center for Molecular Medicine). Cells were grown in RPMI-1640 (SW620 and SW480) or DMEM (HCT116 and Caco-2) medium (Life Technologies) supplemented with 10 % fetal bovine serum (Invitrogen) in an atmosphere of 95 % air and 5 % CO₂ at 37°C. All cells were free of mycoplasma as regularly confirmed with the MycoAlert mycoplasma detection kit (Lonza). Authentication of the cell lines was performed by short tandem repeat (STR) genotyping at the Leibniz-Institut DSMZ (Braunschweig, Germany). STR genotypes were consistent with published genotypes for these cell lines.

Tissue preparation, histology and immunohistochemistry

Mice were sacrificed by cervical dislocation at defined time points (or when showing signs of disease) and the organs were quickly dissected, flushed with cold phosphate-buffered saline (PBS) and fixed overnight in 4% formalin for paraffin embedding, or stored in RNA^{later} (Ambion) for RNA extraction.

For the assessment of macroscopic tumors of the intestine (> 0.5 mm), the intestinal tract was removed immediately after euthanasia, divided into four segments comprising the duodenum, jejunum, ileum and colon, opened longitudinally, rinsed with cold PBS and examined under a dissection microscope. The tumors were counted and measured by two independent researchers (one was blinded for the animals' genotype).

For histological analysis, 3 µm paraffin sections were stained using H&E and scored in a blinded fashion by 2 independent pathologists (W.H. and H.B.).

For immunohistochemistry staining, paraffin sections were rehydrated and antigen retrieval was performed by microwaving the sections in Trilogy Buffer (Cell Marque, Rocklin, CA) or Citrate Buffer (10 mM sodium citrate, pH 6.0). Primary antibodies were rabbit anti-MACC1 (polyclonal,

Sigma-Aldrich), rabbit anti-ki-67 (clone SP6, Thermo Scientific), rabbit anti-collagen IV (polyclonal, Abcam), mouse anti- β -catenin (clone 14, BD Biosciences). Specific binding was detected using Vectastain Elite ABC kit (rabbit IgG), M.O.M. basic kit and DAB substrate (all from Vector laboratories). Incubation times with DAB were equal for all samples. For immunofluorescence, Cy3-conjugated donkey anti-rabbit (Jackson Lab), Cy3-conjugated goat anti-mouse and Alexa Fluor 488-conjugated goat anti-rabbit antibodies (Life Technologies) were used. Nuclei were counterstained with DAPI and pictures were taken with a fluorescence microscope (Axio Observer.Z1 (inverse); Zeiss).

RNA extraction and qRT-PCR

Total RNA was isolated from cells and tissues using GeneMATRIX Universal RNA Purification Kit (Roboklon), according to the manufacturer's instructions. Quantification of RNA concentration was performed with Nanodrop (Pqlab), and total RNA was reverse transcribed with random hexamers in a reaction mix containing 5 mM MgCl₂, 1× RT-buffer, 250 μ M pooled dNTPs, 1 U/ μ L RNase inhibitor and 2.5 U/ μ L Moloney Murine Leukemia Virus reverse transcriptase (all from Applied Biosystems). The reaction occurred at 23°C for 15 minutes, 42°C for 45 minutes, 95°C for 5 minutes, and subsequent cooling at 4°C. The cDNA product was amplified in a total volume of 10 μ L in 96-well plates using the LightCycler 480 (Roche Diagnostics), with SYBR Green (Promega) and the primers listed in Table 2. For cDNA amplification, the following PCR conditions were used: 95°C for 2 minutes, followed by 45 cycles of 95°C for 7 seconds, 60°C for 10 seconds, and 72°C for 5 seconds. To control for primer dimers or unwanted PCR side products the melting curve was measured with a continuous temperature increase from 65°C to 95°C with a rate of 0.1 °C/sec. Mean values were calculated from duplicate qRT-PCR reactions, after normalization to the respective mean amount of the housekeeping gene (hGAPDH or mGAPDH and m36B4) cDNA.

Table 1. Primers for genotyping vil-MACC1 mice

Name	Sequence 5' – 3'	PCR product
Genotyping-for	GCCAATAGAACTGGGCTTGT	177 bp
Genotyping-rev	GTGCAATTCTTCCTGACCGAAA	
beta-globin for	CCAATCTGCTCACACAGGATAGAGAGGGCAGG	494 bp
beta-globin rev	CCTTGAGGCTGTCCAAGTGATTCAGGCCATCG	

Table 2. Primers for qRT-PCR

Primer	Sequence 5' – 3'	PCR product
hGAPDH for	GAAGATGGTGATGGGATTC	226 bp
hGAPDH rev	GAAGGTGAAGGTCGGAGT	
h β -catenin for	GTGCTATCTGTCTGCTCTAGTA	154 bp
h β -catenin rev	CTTCCTGTTTAGTTGCAGCATC	
hMACC1 for	TTCTTTTGATTCCTCCGGTGA	136 bp
hMACC1 rev	ACTCTGATGGGCATGTGCTG	
hNanog for	ATGCCTCACACGGAGACTGT	65 bp
hNanog rev	AGGGCTGTCCTGAATAAGCA	
hOct4 for	ACATCAAAGCTCTGCAGAAAGAAC	126 bp
hOct4 rev	CTGAATACCTTCCCAAATAGAACCC	

m36B4 for	ACCTCCTTCTTCCAGGCTTT	101 bp
m36B4 rev	CCCACCTTGTCTCCAGTCTTT	
mGAPDH for	CATGTTCCAGTATGACTCCACTC	136 bp
mGAPDH rev	GGCCTCACCCCATTTGATGT	
mCD44 for	TCTGCCATCTAGCACTAAGAGC	106 bp
mCD44rev	GTCTGGGTATTGAAAGGTGTAGC	
mc-myc for	TAACTCGAGGAGGAGCTGGA	114 bp
mc-myc rev	GCCAAGGTTGTGAGGTTAGG	
mki-67 for	GCTGTCCTCAAGACAATCATCA	71 bp
mki-67 rev	GGCGTTATCCCAGGAGACT	
mLEF1 for	CCCACACGGACAGTGACCTA	66 bp
mLEF1 rev	TGGGCTCCTGCTCCTTTCT	
mLgr5 for	ACCCGCCAGTCTCCTACATC	197 bp
mLgr5 rev	GCATCTAGGCGCAGGGATTG	
mMMP7 for	CTGCCACTGTCCCAGGAAG	175 bp
mMMP7 rev	GGGAGAGTTTTCCAGTCATGG	
mMMP9 for	CCATGCACTGGGCTTAGATCA	147 bp
mMMP9 rev	GGCCTTGGGTCAGGCTTAGA	
mNanog for	ACCTGAGCTATAAGCAGGTTAAGAC	116 bp
mNanog rev	GTGCTGAGCCCTTCTGAATCAGAC	

mOct4A for	AGTGGAAGCAACTCAGAGG	134 bp
mOct4A rev	AACTGTTCTAGCTCCTTCTGC	
mPLAU for	TACTGCAGGAACCCTGACAAC	104 bp
mPLAU rev	TGCTAAGAGAGCAGTCATGCAC	
mTCF4 for	CACCCGGCCATCGTCACAC	235 bp
mTCF4 rev	GCCACCTGCGCCCGAGAAT	
mTNFRSF19 for	ATTCTCTTCCTACTCCACCTG	151 bp
mTNFRSF19 rev	CATAGCCGAAGCCACATTC	
mVEGFA for	GACGGGCCTCCGAAACCAT	173 bp
mVEGFA rev	ACGGCAGTAGCTTCGCTGGT	

Table 3. Primers for ChIP

Name	Sequence 5' - 3'	PCR product
hNanog ChIP for	GTTCTGTTGCTCGGTTTTCT	95 bp
hNanog ChIP rev	TCCCGTCTACCAGTCTCACC	

Table 4. The 50 most upregulated genes when comparing Apc vs vil-MACC1/ApcMin mice (sorted by log₂ fold change)

geneSymbol	log₂ fold change	p value
Pla2g4c	5,9017367	2,93E-04
Gsdmc3	4,0382395	8,18E-04
Gsdmc2	3,9906654	9,72E-04
Gsdmc4 Gsdmc2	3,9615088	0,0049375
Mcpt1	3,0842686	9,56E-04
Mcpt2	2,7670965	0,0017748
Cpa3	2,7490506	0,0022187
Slc5a12	2,7145886	0,021317
Capn13	2,635768	0,00261964
Mme	2,3661213	0,04184261
Apol10a	2,2154903	0,02225884
Asah2	2,0613003	0,03158233
Oasl2	2,0109253	5,59E-04
G630090E17Rik	1,823206	0,01234099
Rgs13	1,816721	9,83E-04
Oas1g	1,7971845	8,24E-05
Gm5431	1,7753644	0,00215811
Cd7	1,7487268	0,01951447
Cma2	1,6991405	0,00317897
Vnn1	1,6797915	0,00757349
Slc28a1	1,6703463	0,02326121
Ang4	1,6376486	0,00141017
Trim38	1,6123685	0,00143423
Trim30d	1,5913463	0,00378671
Gzmb	1,5488075	0,03651876
Alox5	1,5388283	0,00714748
Nlrp6	1,5227242	0,01178651
Ddx60	1,5068016	0,00535647
Rragd	1,487195	0,03077347
Clca3	1,4463711	0,00329578
Slc13a1	1,4333019	0,0333743
Mcpt-ps1	1,4140215	0,02737925
Otc	1,4029616	0,02412177
Hcn1	1,4011025	0,04326888
Gnpda1	1,3903879	0,01602425
Cd3g	1,3755102	0,02281035
Cyp2u1	1,3746624	0,00182747
Fmo5	1,3488636	0,01243999
Slc10a5	1,3463545	0,0204559
Scin	1,3462105	4,52E-04
Apol7c	1,3405056	0,02200102

Mcpt4	1,3397231	0,01949804
Tubal3	1,3327894	0,01590599
2010003K11Rik	1,3266286	0,00655141
Sh2d7	1,3255099	0,0389512
H2-T3 H2-T3- like LOC100862459 LOC633417 H2- T18	1,3230934	0,01088176
Itln1 Itlnb	1,3199797	0,03084899
Cps1	1,3118477	0,02589518
Rep15	1,3092332	0,00630612
Hsph1	1,3088627	0,00949879

Table 5. The 50 most downregulated genes when comparing Apc vs vil-MACC1/ApcMin mice (sorted by log₂ fold change)

geneSymbol	log ₂ fold change	p value
Bpifb9a	-2,6625876	0,00154309
Ly6g	-2,3405137	0,04494718
Ighg	-2,1479988	0,00955943
Cxcl13	-1,848691	0,00781575
Spock2	-1,7160082	0,01180256
Lcn2	-1,6879044	0,01537303
Myot	-1,67028	0,00299974
Slc7a11	-1,6661639	0,00417117
Cd177	-1,6649876	0,00262086
Saa3	-1,6410255	0,04799187
Pnliprp1	-1,6317042	0,00243124
Nrn1	-1,6181736	0,00986208
S100g	-1,5956593	0,01895532
Hemt1 Gml	-1,5633831	0,00153114
Hbb-b1 Hbb-b2 Beta-s	-1,5224694	0,02275072
Plat	-1,4606122	0,00769508
Rbm11	-1,4515014	0,00719425
Gpcpd1	-1,4451628	0,00237589
Gpr64	-1,4441136	0,00321575
Gml	-1,437985	3,72E-04
Pappa	-1,42731	0,00378457
Pdk4	-1,3776388	0,00399306
Bmyc	-1,3743773	0,00976266
Sema3c	-1,3681793	0,01438862
Cxcl2	-1,3526081	0,00562999
Ier3	-1,33634	0,01996473
1600029D21Rik	-1,3228607	0,04030265
Igfbp1	-1,3222307	0,03074161
2610524H06Rik	-1,3113202	0,01272145

Stc1	-1,3100462	0,01878368
Dusp1	-1,28895	0,00649639
Gm19544	-1,2875785	0,00714845
Fzd10	-1,2832742	0,02326645
Gsdma	-1,2811289	0,00855811
Adm	-1,2507396	0,03708091
Igfbp3	-1,2478275	0,00503722
Apod	-1,2383671	0,0053949
S100a8	-1,2366333	0,00733322
Mt2	-1,2310781	0,00252987
Per1	-1,2253866	0,01898611
Apcdd1	-1,2246275	0,00967644
Snord99	-1,2156476	0,0045955
Lbp	-1,213538	0,02141159
Ppbp	-1,2120585	0,00373943
Notum	-1,2036572	0,04049894
Cyp1b1	-1,193336	6,63E-04
9530003J23Rik	-1,1837797	1,13E-04
Olf920	-1,1749887	0,03616339
2610528A11Rik	-1,1500368	0,02447424
Wfdc15b	-1,1499958	0,03364104
Wif1	-1,1443462	0,04845512
Dkk3	-1,1378593	0,00168533

Supplementary Figure Legends

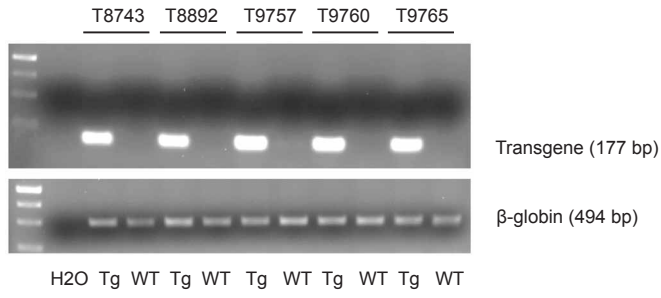
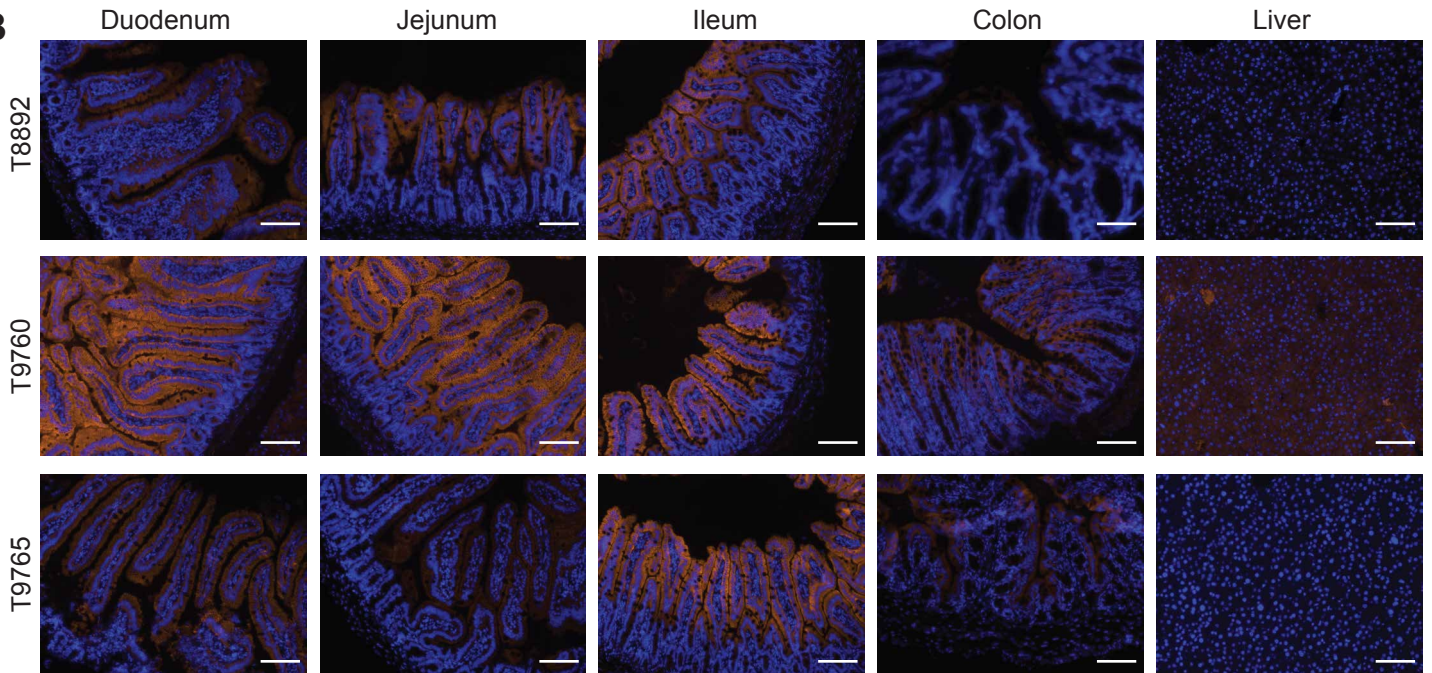
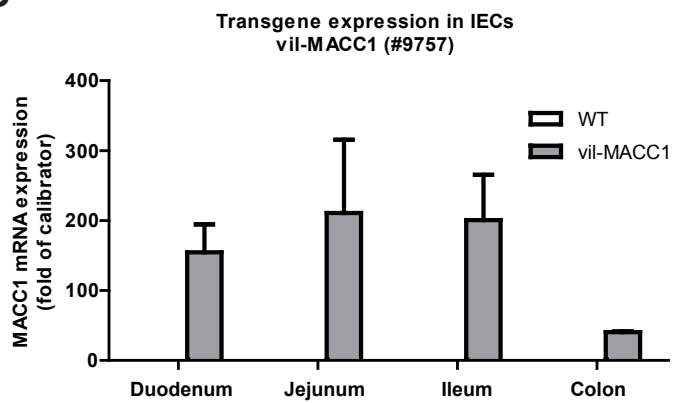
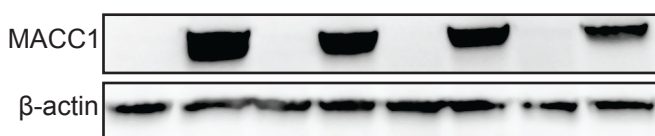
Supplementary Figure 1. Generation of transgenic mice with IEC-specific overexpression of MACC1. (A) Five independent founder lines of vil-MACC1 mice were generated on a pure C57BL/6N background (T8743, T8892, T9757, T9760 and T9765). Mice were genotyped by PCR using transgene-specific (genotyping) primers and mouse beta-globin primers as internal control. (B) Immunofluorescent staining with an anti-MACC1 antibody shows expression of MACC1 in the epithelial cells of the duodenum, jejunum, ileum and colon, but not in the liver of vil-MACC1 mice. The depicted images are representative of 3 different vil-MACC1 lines (line T8892, upper row; line T9760, middle row; line T9765, lower row) with MACC1 stained in red (Cy3) and the nuclei stained in blue (DAPI). Scale bars: 100 μ m. Transgenic MACC1 mRNA (C) and protein (D) were specifically detected in the intestinal epithelial cells (IECs) of vil-MACC1 mice (T9757). mRNA data represent mean \pm SEM ($n = 2$).

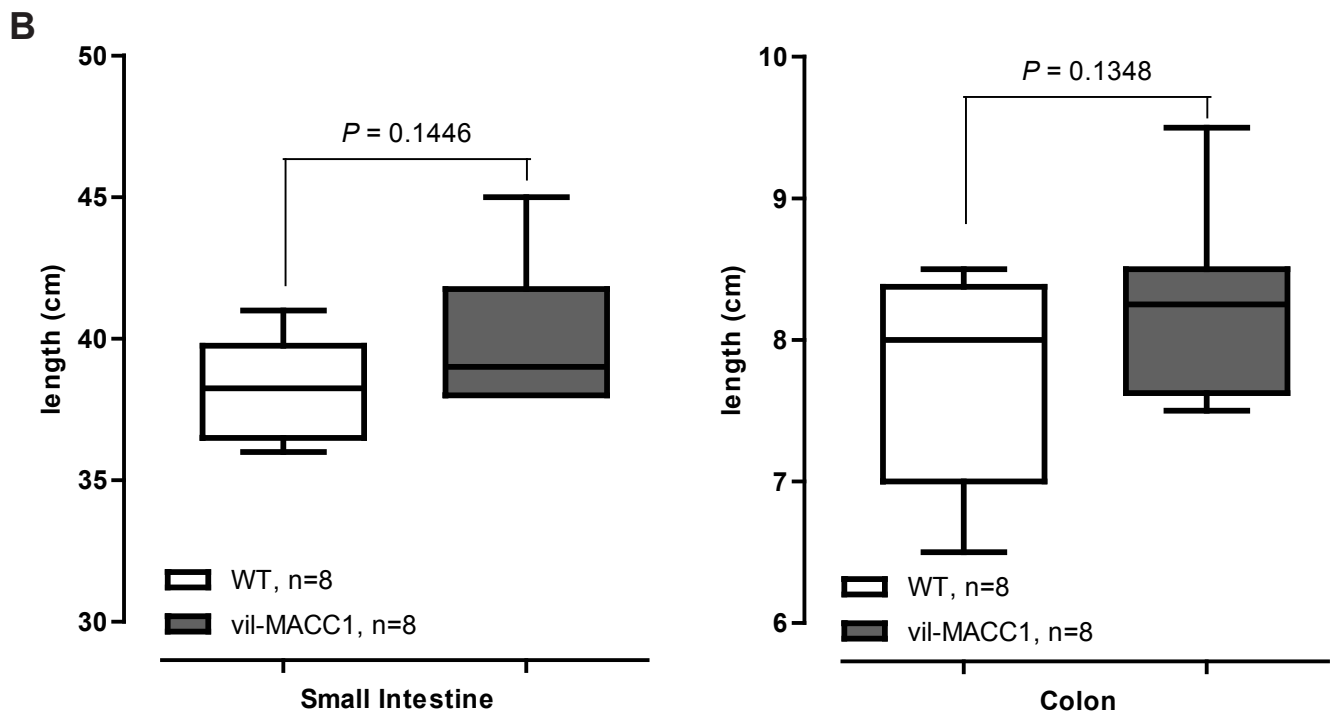
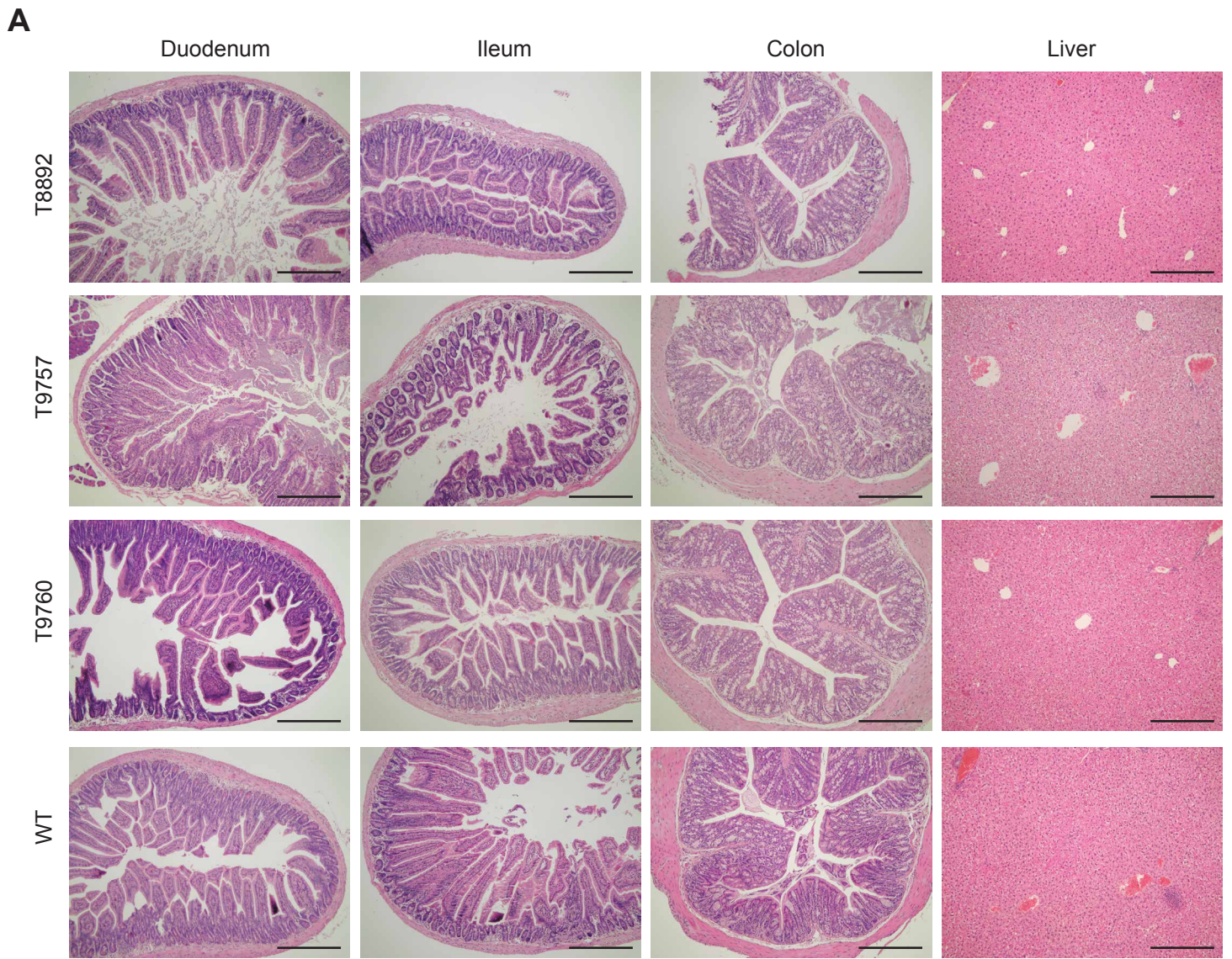
Supplementary Figure 2. Characterization of the vil-MACC1 transgenic mice. (A) Histological analysis of the SI, colon and liver of young (3-months old) vil-MACC1 mice revealed the absence of abnormalities in these animals as compared with WT control littermates. Scale bars: 100 μ m (B) Three-months old vil-MACC1 mice had a similar length of the SI and colon as their littermate controls ($n = 8$, per genotype). P values were calculated using unpaired two-tailed Student's t test with Welch's correction. (C) Aged (≥ 1 year) vil-MACC1 mice developed intestinal tumors at a very low rate ($< 20\%$). Depicted are representative H&E pictures of 2 jejunal adenomas. Scale bars: 100 μ m (left image) and 50 μ m (right image). (D) A similar length of the SI and colon was also found in aged vil-MACC1 mice as compared with WT littermate controls ($n = 12$, per genotype). P values were calculated using unpaired two-tailed Student's t test with Welch's correction.

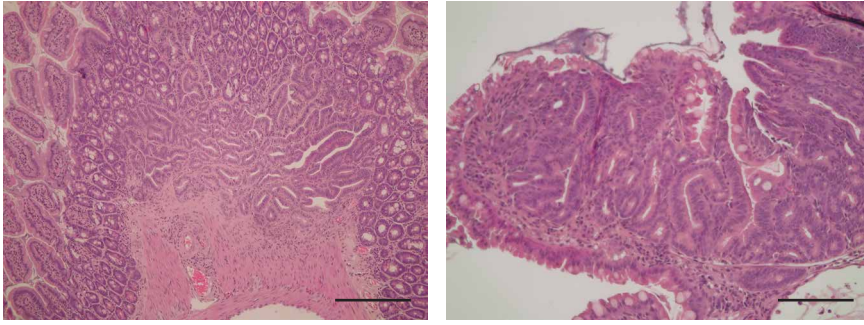
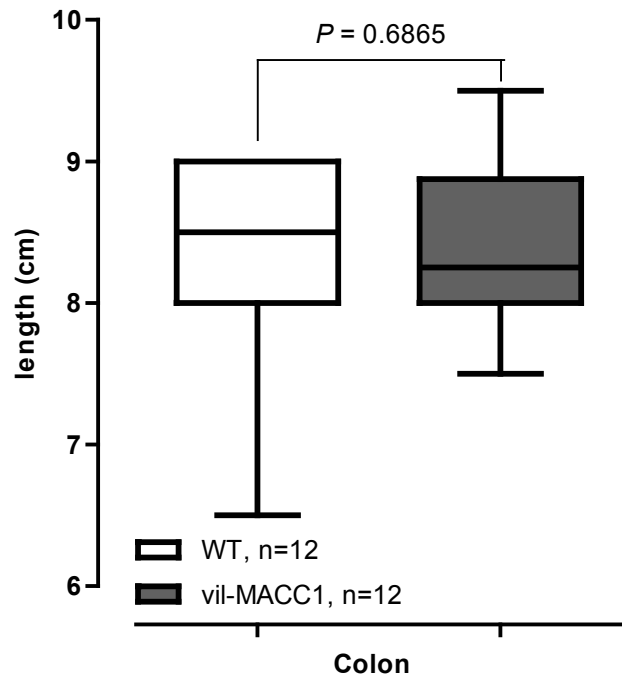
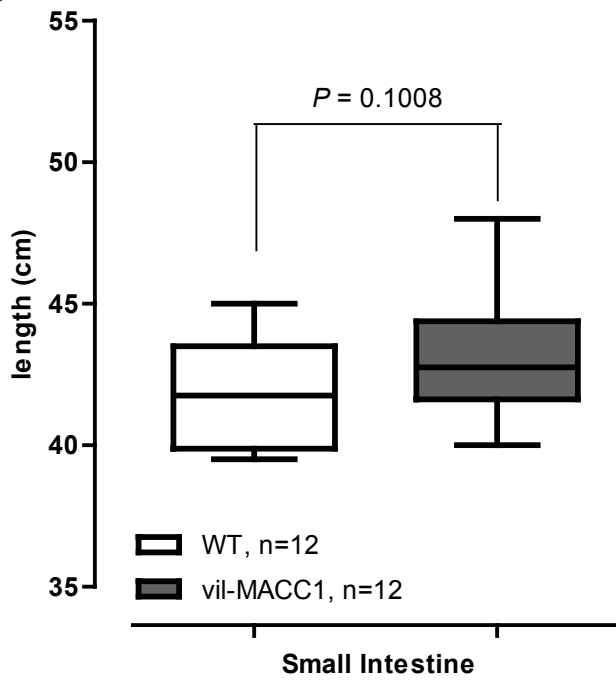
Supplementary Figure 3. MACC1 transgene expression in the vil-MACC1/Apc^{Min} mice. (A) qRT-PCR analysis revealed transgenic MACC1 mRNA expression in the duodenum, jejunum, ileum and colon, but not in the liver of vil-MACC1 and vil-MACC1/Apc^{Min} transgenic lines. In addition, transgenic MACC1 was also expressed in the tumors of the small and large intestine of vil-MACC1/Apc^{Min} mice. Data represent mean \pm SEM ($n \geq 4$, per genotype). (B) Immunofluorescent staining with an anti-MACC1 antibody shows expression of MACC1 in the epithelial cells of the duodenum, jejunum, ileum, colon and tumor tissue of vil-MACC1/Apc^{Min} mice. The depicted images are representative of Apc^{Min} (lower row) and vil-MACC1/Apc^{Min} (upper row) mice with MACC1 stained in red (Cy3) and the nuclei stained in blue (DAPI). Scale bars: 100 μ m.

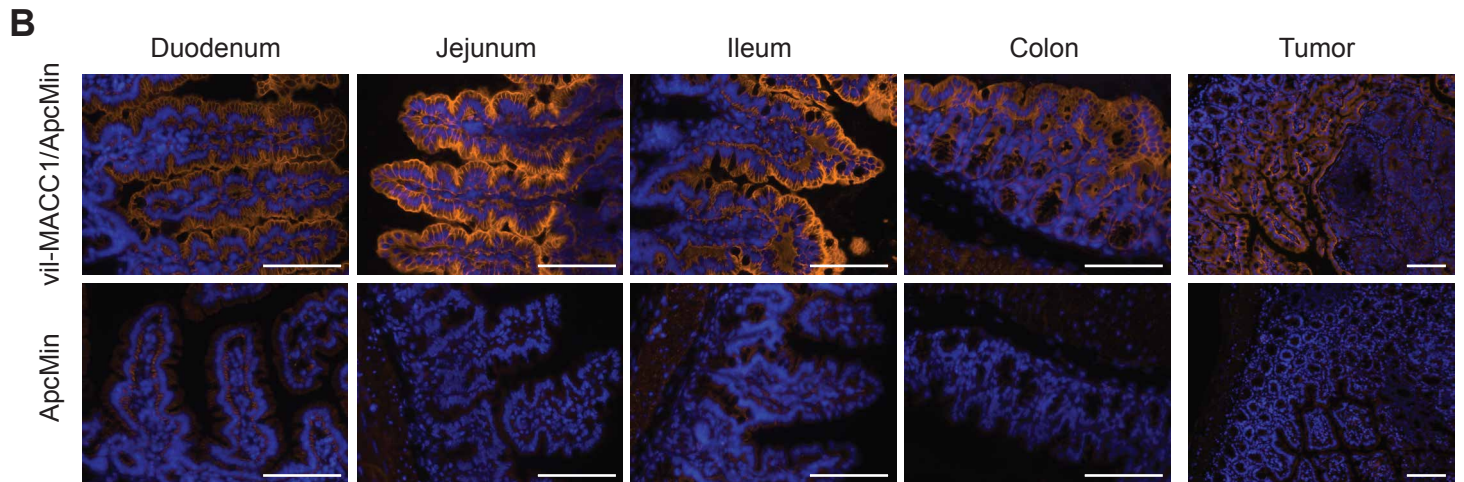
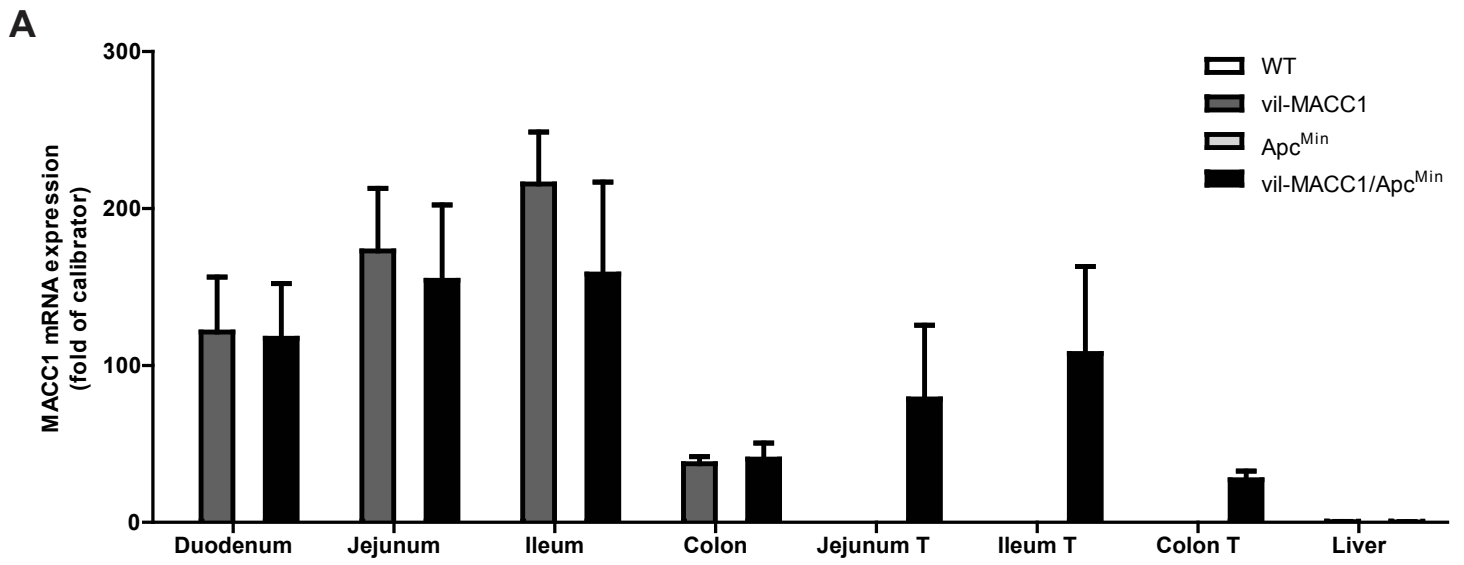
Supplementary Figure 4. Characterization of the vil-MACC1/Apc^{Min} mice. (A) At the age of 17 \pm 2 weeks, the vil-MACC1/Apc^{Min} mice showed a non-significant small increase in the total number of intestinal tumors. Quantification was performed by 2 independent researchers for vil-MACC1/Apc^{Min} and Apc^{Min} ($n = 9$, per genotype) control mice. *P* values were calculated using unpaired two-tailed Student's *t* test with Welch's correction. (B) A strong and significant positive correlation was found between the spleen size (determined as % of body weight) and the total number of intestinal tumors in vil-MACC1/Apc^{Min} and Apc^{Min} mice. Correlation analysis was performed with non-parametric Spearman's correlation. (C) Apc^{Min} mice display an increased spleen size (% bw) as compared with WT and vil-MACC1 mice, a phenotype that is further exacerbated in vil-MACC1/Apc^{Min} mice. Analysis was performed in mice at 25 \pm 2 weeks of age (WT, $n = 7$; vil-MACC1, $n = 9$; Apc^{Min}, $n = 10$; vil-MACC1/Apc^{Min}, $n = 14$). Transversal bars represent the mean. (D) Representative pictures of the spleen of WT, Apc^{Min} and vil-MACC1/Apc^{Min} mice showing the presence of splenomegaly in the latter two.

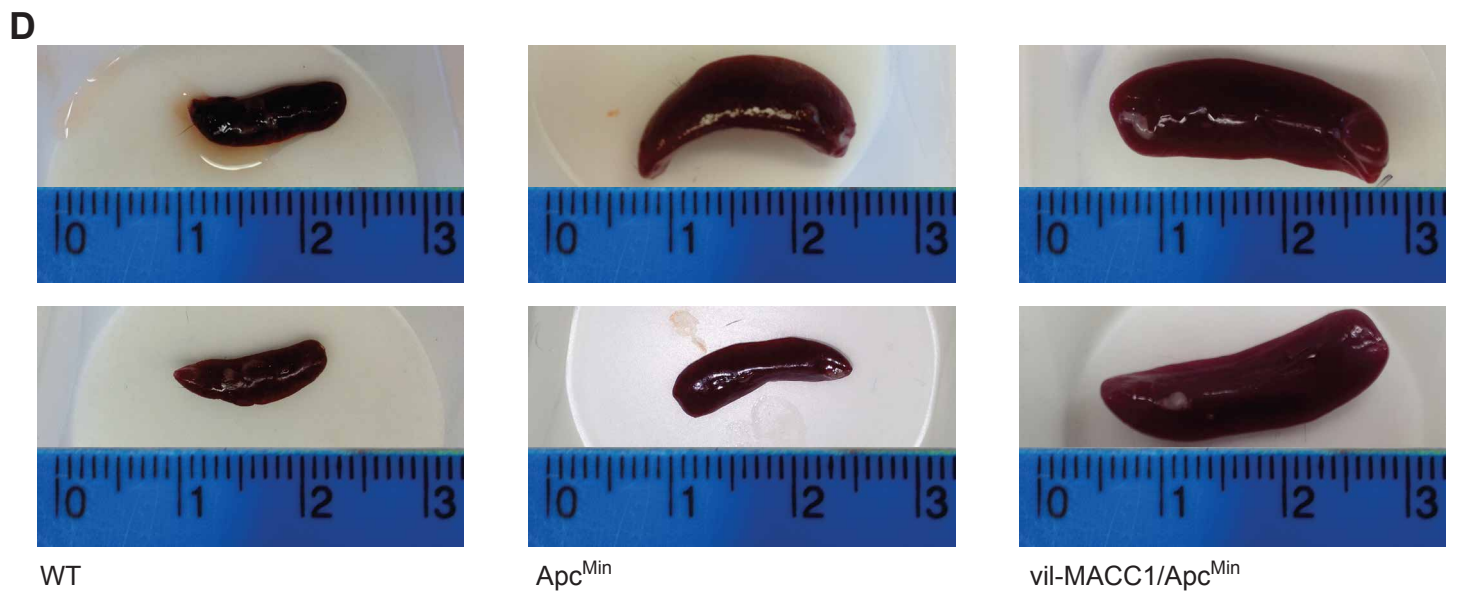
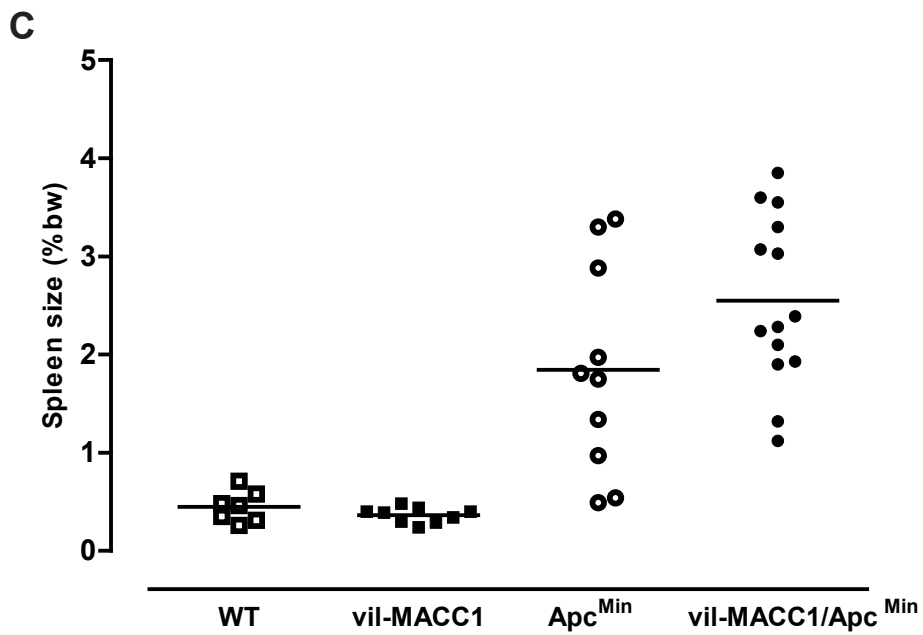
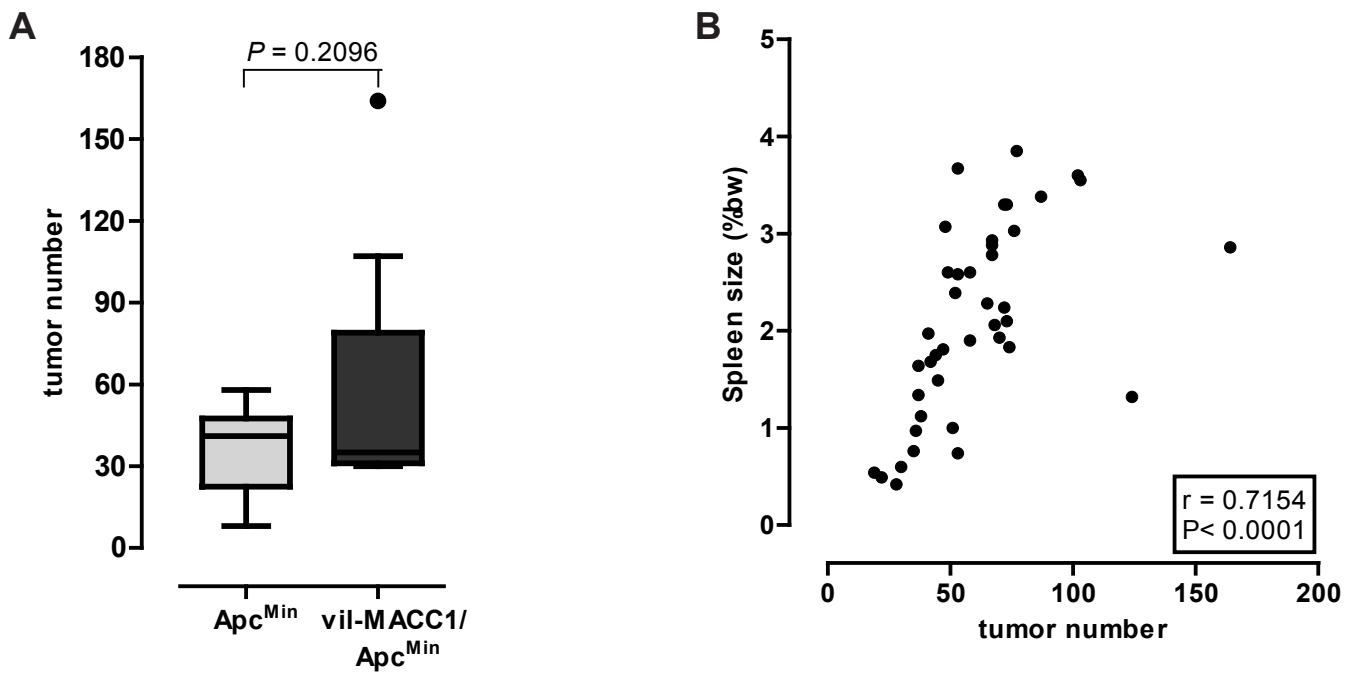
Supplementary Figure 5. Pathway analysis of the Affymetrix microarray. Pathway analysis identified the Wnt pathway and pluripotency as significantly upregulated in the SI tumors of vil-MACC1/Apc^{Min} mice as compared with Apc^{Min} control animals. Highlighted in yellow are the genes with a statistically significant increase in the former compared with the latter.

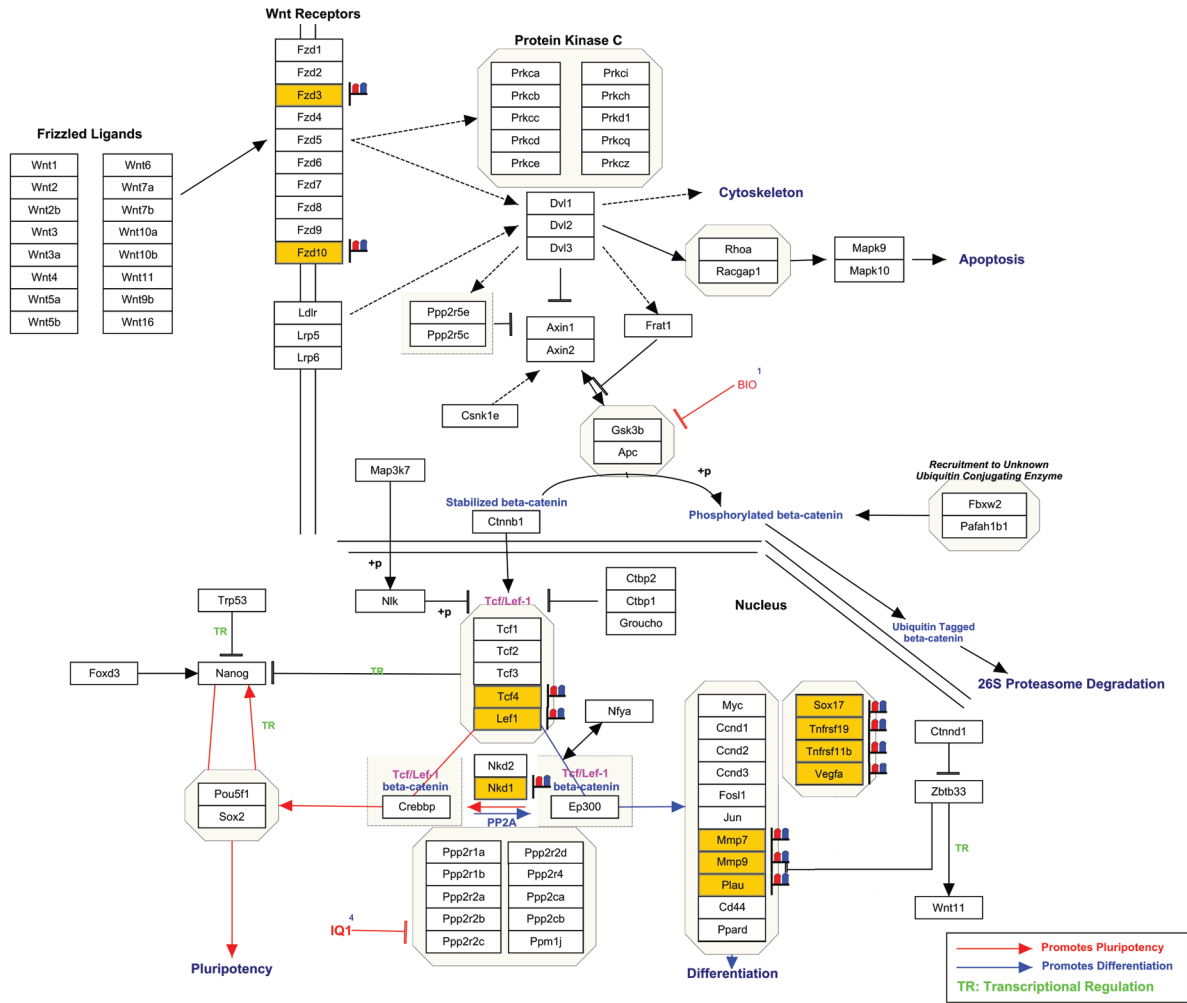
A**B****C****D**



C**D**







Supplementary Figure 5
Lemos, Hardt et al. 2015